IS-T- 894

Flux-line-cutting threshold in type II superconductors

by

Ying-Cheun Spring Yeh

MS Thesis submitted to Iowa State University

Ames Laboratory, DOE

Iowa State University

Ames, Iowa 50011

Date Transmitted: March 1980

PREPARED FOR THE U.S. DEPARTMENT OF ENERGY
UNDER CONTRACT NO. W-7405-eng-82

DISCLAIMER

IS-T-894

Flux-line-cutting threshold in type II superconductors

by

Ying-Cheun Spring Yeh

A Thesis Submitted to the

Graduate Faculty in Partial Fulfillment of the

Requirements for the Degree of

MASTER OF SCIENCE

Department: Physics
Major: Solid State Physics

Approved:

John M. Clem
In Charge of Major Work

For the Major Department

For the Graduate College

Iowa State University
Ames, Iowa

1979

DISCLAIMER

Printed in the United States of America

Available from
National Technical Information Service
U.S. Department of Commerce
5265 Port Royal Road
Springfield, VA 22161

TABLE OF CONTENTS

LIST OF SYMBOLS

$f_+(f_-)$	net force per unit length of vortex exerted on a right (left) - displaced vortex
f_{+n}	force per unit length of vortex exerted on a right-displaced vortex by the left-displaced vortices in plane n at $-x + nD_\perp$
λ	weak-field penetration depth
λ_B	field-dependent penetration depth
ξ	weak-field coherence length
ξ_B	field-dependent coherence length
ξ_v	weak-field variational core radius parameter
ξ_{vB}	field-dependent variational core radius parameter
b	vortex density in reduced units
$\Delta\alpha_c$	critical angle for flux-line cutting
$\Delta\alpha_{co}$	critical angle for instability at the origin
$\Delta\alpha_{cm}$	critical angle for flux-line cutting (smallest angle for which $f_+ \geq 0$ for all $0 \leq x \leq D_\perp/2$)
$\tilde{k}_c$	critical angle gradient in reduced units
$\tilde{j}_{c\parallel}$	longitudinal critical current density in reduced units

CHAPTER I. INTRODUCTION

The electrodynamic behavior of a current-carrying type II superconducting wire subjected to a longitudinal magnetic field is still not completely understood, despite a large number of experimental and theoretical investigations.[1-27] Above a certain critical current I_c, a longitudinal voltage accompanied by a paramagnetic moment has been observed.[12,14,21,22] A macroscopic theory of a nearly force-free arrangement of helical vortices[2,12] has been developed which can account for the moment but not for the voltage. The voltage produced cannot be described as a flux-flow voltage generated by an inward-collapsing array of helical vortices, because this would lead to an ever-increasing buildup of longitudinal magnetic flux.[12,13,18,19] Flux-line cutting[12,16,23,26] (the intersection and cross-joining of adjacent nonparallel vortices) has been proposed as a mechanism to explain the coexistence of the voltage and the moment. A description by Walmsley[12,16] suggests that the flux lines can be split up and rejoined in such a way that the azimuthal component of the flux moves radially in towards the axis while the axial component remains static.

Clem[23] proposed a model to explain the simultaneous appearance of the voltage and the moment. In his description, helical vortices periodically nucleate at the surface, and as they move inwards they cause the initially existing longer pitch vortices to experience spiral-vortex-expansion instabilities. Flux-line-cutting processes occur, and helical vortices of intermediate pitch are produced, some of which exit at the surface. If, on the average, there are equal numbers of exiting and entering vortices,

a steady-state voltage is produced, while the averaged longitudinal moment remains unchanged.

A specific cyclic flux-line-cutting model was presented in reference 27 for slab geometry. In this model, an infinite superconducting slab of finite width w, oriented perpendicular to the x axis and subjected to an applied field and current in the z direction, as shown in Figure 1, is considered. Planes of parallel vortices are assumed to form a vortex array similar in some respects to that shown in Figure 2. In each plane, vortices are parallel to the net local field. A plane of vortices entering from a surface at $x = \pm w/2$ moves inwards, where it meets another vortex plane with smaller angle between the vortices and the z axis. After flux-line cutting, a plane of intermediate tilt angle is formed, which separates into two planes, one of which exits at the surface. Similar motions allow pairs of vortex planes deeper in the slab simultaneously to undergo flux-line cutting. In steady state, fluxoid conservation dictates that, although no net z flux is transported, a net y flux is transported across the slab in the x direction.[27] By Faraday's law, a nonvanishing time-averaged electric field (or a voltage) in the z direction is produced. The model also permits the calculation of the magnetic flux density, the macroscopic electric current density, and the paramagnetic moment.

For simplicity, the above model assumes that flux-line cutting occurs spontaneously. That is, no critical angle difference between the vortices in adjacent planes needs to be exceeded for flux-line cutting to occur. However, a threshold value for the angle difference is implied in Brandt, Clem, and Walmsley's work.[26] For small angles, the structure might remain

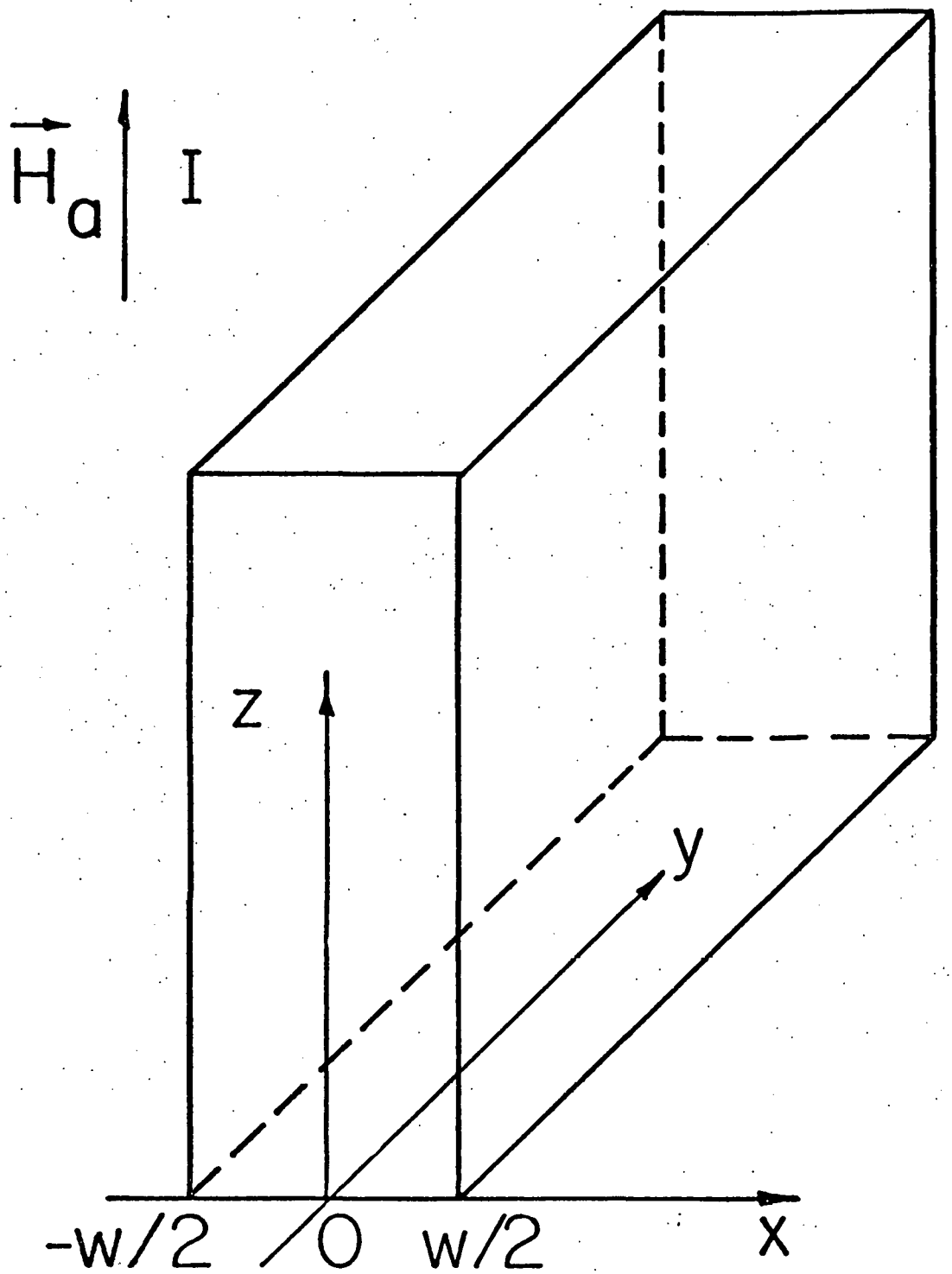

Figure 1. Infinite superconducting slab of width w, oriented perpendicular to the x axis and subjected to an applied field and current in the z direction.

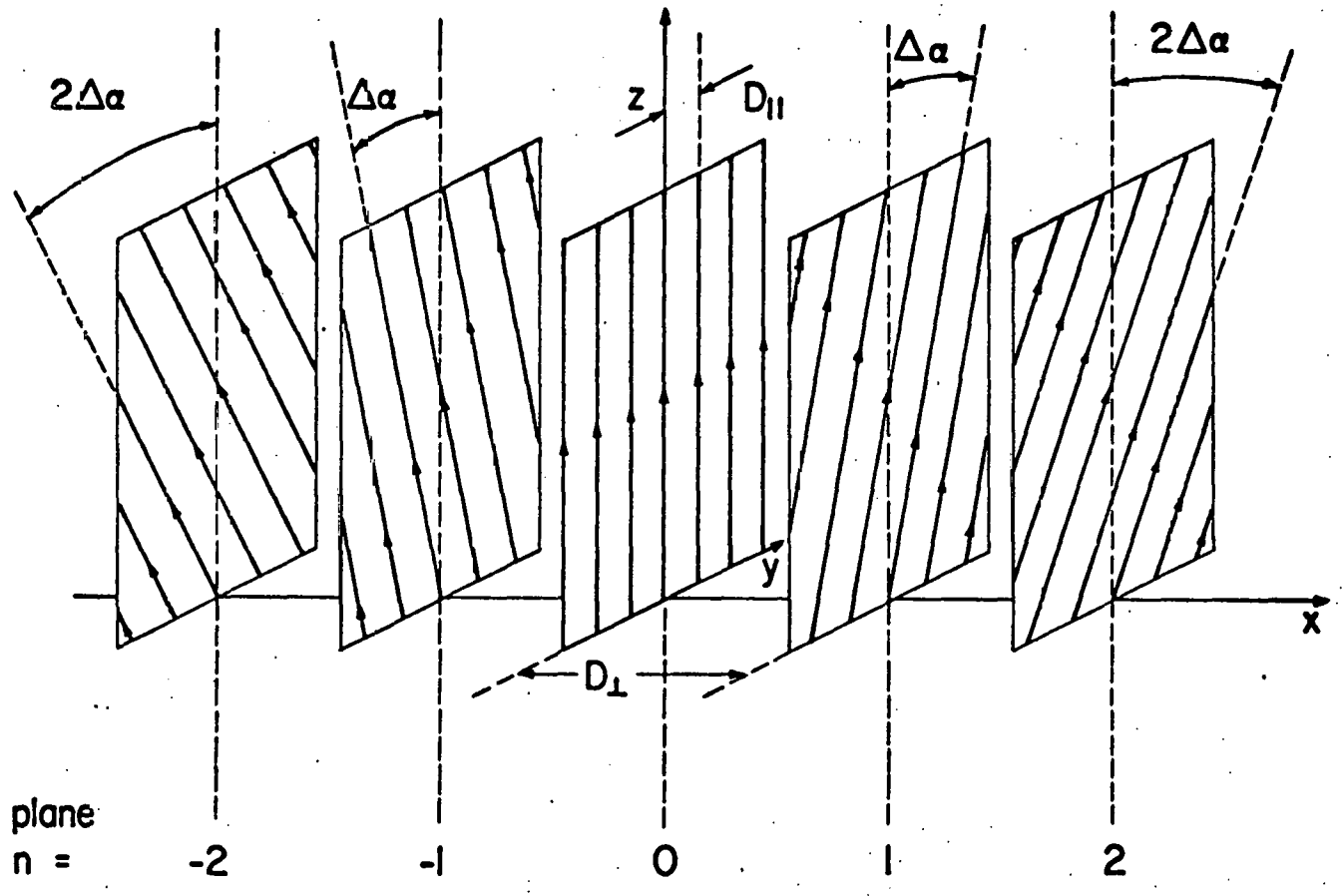

Figure 2. Infinite array of vortex planes whose instability is investigated in this thesis. The intervortex spacing in each plane is $D_\perp$, the intraplanar spacing is $D_\parallel$, and the angle between vortices in adjacent planes is $\Delta\alpha$. (Scale is greatly expanded in x direction.)

in metastable equilibrium, but at higher angles the structure might undergo spontaneous flux-line cutting.

In order to interpret magnetization and a.c. loss measurements in hysteretic superconducting specimens containing nonparallel vortices with different angles, LeBlanc and co-workers[28-31] proposed the existence of a critical angle gradient, analogous to the critical current density in the critical state model. It is possible that such a quantity has its explanation in flux-line cutting, which would redistribute magnetic flux until the angle gradient becomes equal to the critical angle gradient.

The purpose of this thesis is to investigate the threshold for flux-line cutting in slab geometry. In the second chapter of this thesis, a mathematical model, based on the London model and the Ginzburg-Landau theory, for calculating the force on a test vortex in the vortex array is presented. The parameters to be used and some electromagnetic properties are described briefly. An instability analysis is given and the determination of the threshold value for the interplanar angle difference is discussed. Chapter III presents numerical calculations of the forces and critical angles where the Newton's method is employed. Chapter IV shows the results of calculations for forces, critical angles, critical angle gradients, and critical current densities. The dependence of the critical angle upon the vortex density and the intervortex and interplanar spacings is also examined. The significance of the results and conclusions is given in Chapter V.

CHAPTER II. MATHEMATICAL MODEL

In the limit that the penetration depth λ is much large than the coherence length ξ ($\lambda >> \xi$), it is found that the flux density $\vec{h}(r)$ and self-energy ε_s associated with an isolated straight vortex directed along the z-axis are given approximately by[32]

$$\vec{h}(r) = (\phi_0/2\pi\lambda^2)K_0(r/\lambda)\hat{z} \tag{2-1}$$

and

$$\varepsilon_s = (\phi_0/4\pi\lambda)^2 \ln(r/\xi) \tag{2-2}$$

where r is the radial coordinate in cylindrical coordinates, K_0 is the modified Bessel function of order zero and $\phi_0 = hc/2e = 2.07 \times 10^{-7}$ G-cm^2 is the flux quantum. For two parallel straight vortices with separation s and tilt angle $\Delta\alpha$ as shown in Figure 3 the interaction energy per unit length of vortex can be derived as[26]

$$\varepsilon_L(\Delta\alpha, s) = (\phi_0^2/8\pi^2\lambda^2)K_0(s/\lambda) \cos \Delta\alpha \tag{2-3}$$

Integrated along the line element, dy/sin α, the interaction energy becomes

$$E_{em}(\Delta\alpha, s) = (\phi_0^2/8\pi\lambda) \cot \Delta\alpha \cdot \exp(-s/\lambda) \tag{2-4}$$

which is valid provided $\Delta\alpha \neq 0$. When $\Delta\alpha = 0$, from (2-3) the interaction energy per unit length is

$$\varepsilon_{em}(0, s) = (\phi_0^2/8\pi^2\lambda^2)K_0(s/\lambda) \tag{2-5}$$

The interaction energies in Eqs. (2-4) and (2-5) are electromagnetic in nature.

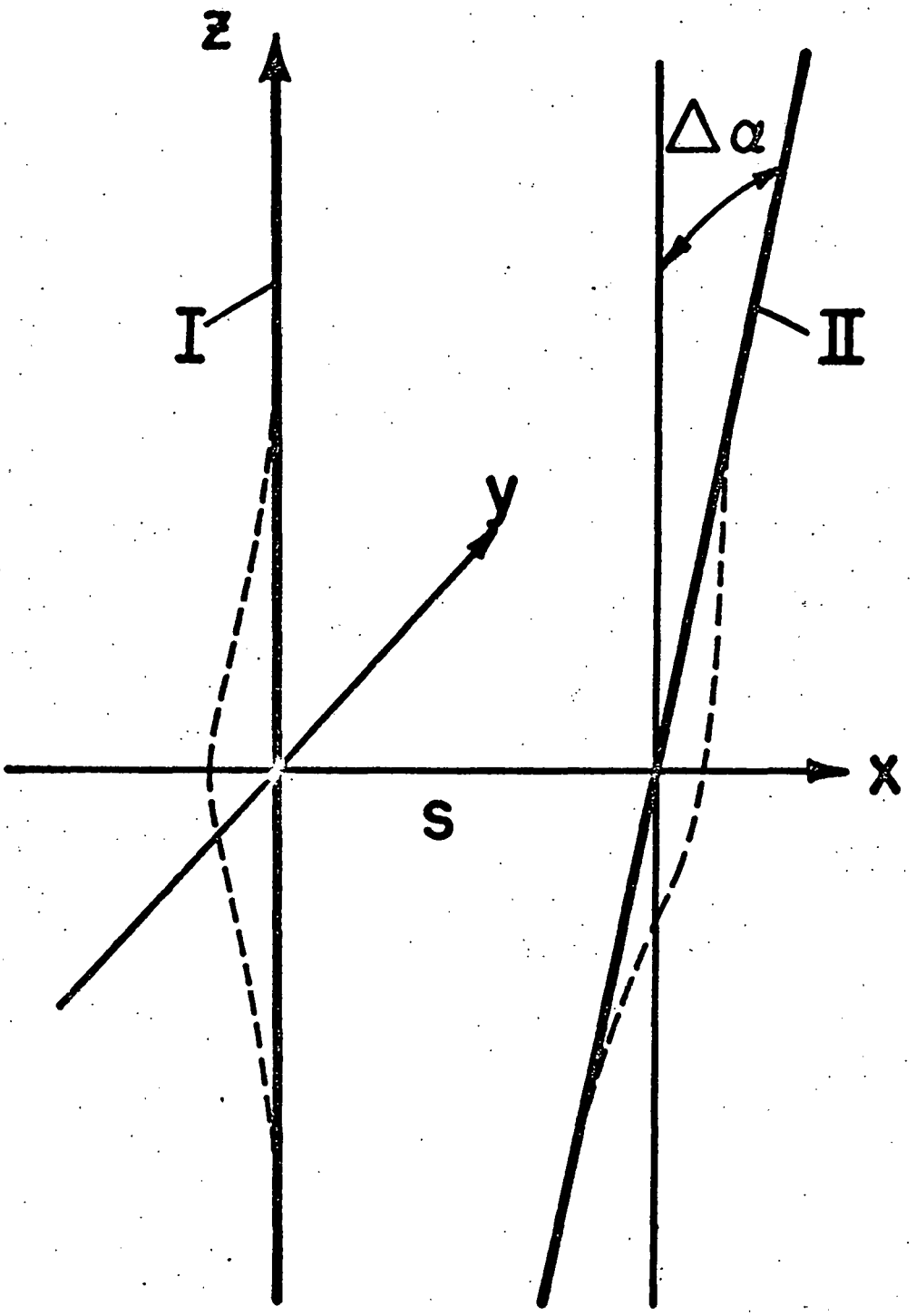

Figure 3. Two parallel straight vortices with separation s and tilt angle $\Delta\alpha$.

In an approximation to the Ginzburg-Landau theory, an attractive "condensation energy" or "core energy" is included in the interaction energy between two parallel straight vortices. For $\Delta\alpha = 0$, its magnitude is[26]

$$V_c(0, s) = -(\phi_0^2/8\pi^2\lambda^2)K_0(s\sqrt{2}/\xi) \tag{2-6}$$

per unit length. From Eqs. (2-3) and (2-7), for $\Delta\alpha = 0$, the total interaction energy per unit length is

$$\varepsilon(0,s) = (\phi_0^2/8\pi^2\lambda^2)[K_0(s/\lambda) - K_0(s\sqrt{2}/\xi)] \tag{2-7}$$

which vanishes when $\kappa = 1/\sqrt{2}$ as expected. Here κ is the Ginzburg-Landau parameter defined to be the ratio λ/ξ. Eq. (2-7) gives rise to a force per unit length as

$$\begin{aligned} f(0, s) &= -\partial\varepsilon(0, s)/\partial s \\ &= (\phi_0^2/8\pi^2\lambda^3) \cdot [K_1(s/\lambda) - \sqrt{2}\,\kappa\, K_1(s\sqrt{2}/\xi)] \end{aligned} \tag{2-8}$$

For $\Delta\alpha \neq 0$, the core interaction energy per unit length is similar to Eq. (2-3) with $\Delta\alpha = 0$ and λ replaced by $\xi/\sqrt{2}$. Integrated along the line element, the interaction energy becomes

$$V_c(\Delta\alpha, s) = -[(\phi_0^2/8\pi\lambda \sin\Delta\alpha)/\sqrt{2}\,\kappa] \exp(-s\sqrt{2}/\xi) \tag{2-9}$$

From Eqs. (2-4) and (2-9), the total interaction energy becomes

$$E(\Delta\alpha, s) = (\phi_0^2/8\pi\lambda \sin\Delta\alpha)\cdot[\cos\Delta\alpha \exp(-s/\lambda) - (\sqrt{2}\kappa)^{-1}\exp(-s\sqrt{2}/\xi)] \tag{2-10}$$

which gives rise to a force

$$F(\Delta\alpha, s) = (\phi_0^2/8\pi\lambda^2 \sin\Delta\alpha)[\cos\Delta\alpha \exp(-s/\lambda) - \exp(-s\sqrt{2}/\xi)] \tag{2-11}$$

At s = 0, Eq. (2-11) shows a cusp, in contradiction to the expected result that the force decreases continuously to zero over the fluxline core radius. The expressions for the forces in Eqs. (2-8) and (2-11) are only approximations in the limit of vanishing core radius. By introducing a core radius parameter ξ_v [26,33] the cusp of the force at s = 0 can be smeared out. The value of ξ_v is found by a variational method that minimizes the free energy. It satisfies

$$\kappa = (\sqrt{2}\lambda/\xi_v)[1 - K_0^2(\xi_v/\lambda)/K_0^2(\xi_v/\lambda)]^{1/2} \tag{2-12}$$

Then Eq. (2-12) becomes

$$F(\Delta\alpha, S) = [A\phi_0^2/(8\pi\lambda^2 \sin \Delta\alpha)][\cos \Delta\alpha \exp(-S/\lambda) - \exp(-S\sqrt{2}/\xi)]\frac{s}{S} \tag{2-13}$$

where

$$S = (s^2 + \xi_v^2)^{1/2}$$

and

$$A = (\lambda/\xi_v)/K_1(\xi_v/\lambda)$$

which is a normalizing constant. Eq. (2-7) is modified in the same way which gives

$$f(0, S) = [A\phi_0^2/(8\pi^2\lambda^3)][K_1(S/\lambda) - \sqrt{2}\,\kappa\, K_1(S\sqrt{2}/\xi)]\,\frac{s}{S} \tag{2-14}$$

At larger induction or smaller κ, say $b = B/H_{c2} > 0.3$ or $\kappa < 2$ where B is the magnetic induction, the vortex cores overlap and the London model fails. It has been shown that[34-37] λ and ξ should be replaced by field-dependent quantities such that the repulsive part of the force field varies over a range of $\lambda_B = \lambda/(1 - b)^{1/2}$ and the attractive part varies over a range of $\xi_B = \xi/(1 - b)^{1/2}$. Accordingly, we in addition replace the core radius parameter by $\xi_{vB} = \xi_v/(1 - b)^{1/2}$.

In the vortex state, the interaction between the vortices leads to a periodic lattice structure when $\Delta\alpha = 0$. It has been found that the triangular lattice usually has minimum free energy.[38] For the type II superconducting slab described in Chapter I, however, the vortices do not form a perfect lattice but instead must have an arrangement similar to that of the model array of Figure 2. In this model, the vortices in plane n at $x_n = nD_\perp$ point in the direction of the unit vector $\hat{\phi}_n = \hat{z} \cos \alpha_n + \hat{y} \sin \alpha_n$ where $\alpha_n = n\Delta\alpha$.

The macroscopic flux density and current distributions generated by this array can be calculated as follows. The flux density contribution of vortex plane n averaged over a distance $D_\parallel$ parallel to the plane and perpendicular to $\hat{\phi}_n$ is approximated by

$$\vec{b}_n(x) = \hat{\phi}_n(\phi_0/2\lambda_B D_\parallel)\exp(-|x - x_n|/\lambda_B) \tag{2-15}$$

The vector sum of contributions from all vortex planes is

$$\vec{b}(x) = \sum_n \vec{b}_n(x) \tag{2-16}$$

The macroscopic $\vec{B}(x)$, the average of $\vec{b}(x)$ over several interplanar separation $D_\perp$, is most conveniently evaluated by converting the sum in Eq. (2-16) to an integral over n, which yields

$$\vec{B}(x) = B_0\hat{\phi}(x)/[1 + (k\lambda_B)^2] \tag{2-17}$$

Here, $\hat{\phi}(x) = \hat{z} \cos kx + \hat{y} \sin kx$, $k = \Delta\alpha/D_\perp$ and $B_0 = \phi_0/D_\parallel D_\perp$, which is the average flux density when $\Delta\alpha = 0$. The corresponding macroscopic averaged supercurrent density is

$$\bar{\vec{j}}(x) = (c/4\pi)\nabla x\vec{B}$$

$$= (ck/4\pi)\vec{B}(x) \qquad (2\text{-}18)$$

Macroscopically, the array appears to be in equilibium, because the macroscopic Lorentz force density vanishes ($\bar{\vec{j}} \times \vec{B}/c = 0$), and the array can be said to be force free. Moreover, the array appears to be microscopically in equilibrium, because on each vortex axis, the local current density $\vec{j}$ generated by all the other vortices is parallel to the axis, such that $\vec{j} \times \vec{\phi}_0/c = 0$. However, the array can be perturbed by thermally induced fluctuations, which propagate through the medium and lead the array away from the force-free configuration.

Sketched in Figure 4 is the perturbation considered in this thesis. Alternate vortices in each of the planes are assumed to be displaced to new positions (solid circles) a distance $x < D_\perp/2$ from their initial positions (+); the remaining vortices are assumed to be displaced in the opposite direction to new positions (open circles) a distance x from their initial positions (+).

The force $f_+(x)$ per unit length of vortex exerted on a right-displaced vortex, say, vortex a in Figure 4, can be calculated by generalizing the force between two vortices to forces from vortex planes.

For $\Delta\alpha \neq 0$, the force $f(\Delta\alpha, S_B)$ per unit length of vortex exerted on a vortex by a plane of vortices of separation $d_\parallel$ is obtained from Eq. (2-13) which gives

$$f(\Delta\alpha, S_B) = F(\Delta\alpha, S_B)/L \qquad (2\text{-}19)$$

$$= (A\phi_0^2/8\pi\lambda_B^2 d_\parallel)[\cos\Delta\alpha \exp(-S_B/\lambda_B) - \exp(-S_B\sqrt{2}/\xi_B)]\frac{s}{S_B} \qquad (2\text{-}20)$$

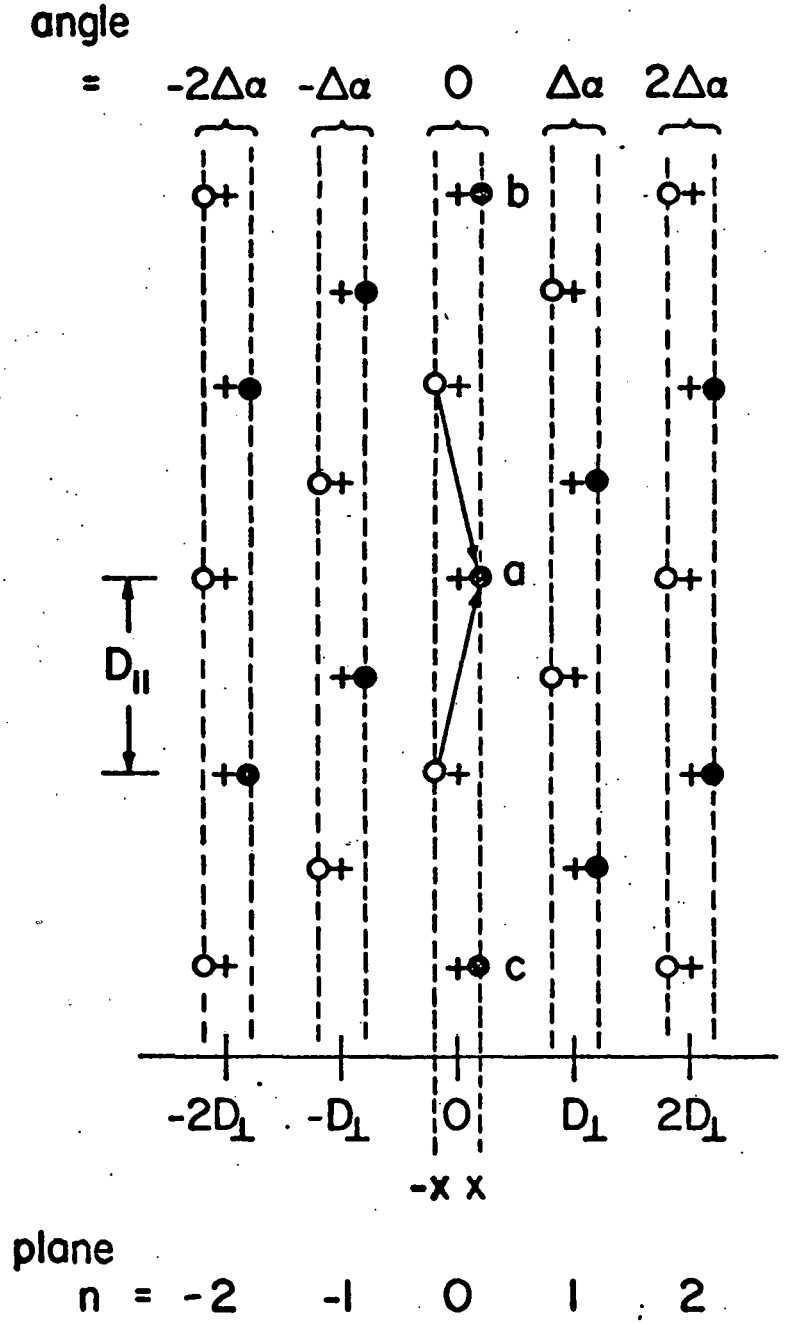

Figure 4. Sketch of perturbation whose instability is investigated in this thesis. Starting from initial positions (+), half the vortices move through +x to new positions (solid circles) and half move through -x to new positions (open circles). Repulsive interaction between vortices (arrows) can lead to unbalanced destabilizing forces.

where $L = d_{\|} / \sin \Delta\alpha$ and $S_B = (s^2 + \xi_{vB}^2)^{1/2}$. For $\Delta\alpha = 0$, the force per unit length of vortex is given by Eq. (2-14), i.e.,

$$f(0, S_B) = (A\phi_0^2/8\pi^2\lambda_B^3)[K_1(S_B/\lambda_B) - \sqrt{2}\,\kappa\, K_1(S_B\sqrt{2}/\xi_B)]\frac{s}{S_B} \tag{2-21}$$

where the field-dependent λ_B has been used.

Now, consider the force $f_+(x)$. The vector sum of the forces from vortices b and c at distance $2D_{\|}$ from vortex a vanishes by symmetry, as do all similar vector sums of the forces from pairs of in-plane vortices. The vector sum of the forces from the two planes of right-displaced vortices at distance $D_\perp$ to the right and to the left of vortex a also vanishes by symmetry, as do all similar sums of forces from pairs of vortex planes. Therefore

$$f_+(x) = \sum_{n=-\infty}^{\infty} f_{+n}(x) \tag{2-22}$$

where $f_{+n}(x)$ is the force in the x direction per unit length of vortex exerted by all left-displaced vortices in plane n. For n = 0, we obtain from Eq. (2-22)

$$f_{+0}(x) = (A\phi_0^2/2\pi^2\lambda_B^3) \sum_{m=1}^{\infty} [K_1(S_{mB}/\lambda_B) - \kappa\sqrt{2}K_1(S_{mB}\sqrt{2}/\xi_B)]x/S_{mB} \tag{2-23}$$

where

$$S_{mB} = \{(2x)^2 + [(2m - 1)D_{\|}]^2 + \xi_{vB}^2\}^{1/2}$$

and, for $n \neq 0$, we obtain from Eq. (2-20)

$$f_{+n}(x) = (A\phi_0^2/16\pi\lambda_B^2 D_{\|})[\cos(n\Delta\alpha)\exp(-X_{nB}/\lambda_B) - \exp(-X_{nB}\sqrt{2}/\xi_B)] \cdot (2x - nD_\perp)/X_{nB} \tag{2-24}$$

where

$$X_{nB} = [(2x - nD_\perp)^2 + \xi_{vB}^2]^{1/2}$$

Although the force $f_+(x)$ is calculated for vortex a in Figure 4, the net force is the same for any right-displaced vortex by symmetry. Moreover, the net force $f_-(x)$ in the x direction per unit length of vortex exerted on a left-displaced vortex as shown by open circles in Figure 4 obeys $f_-(x) = -f_+(x)$.

The stability of the vortex array against the perturbation of Figure 4 depends upon the sign of $f_+(x)$. If $f_+ < 0$ for small x, the structure is stable to small perturbations; if $f_+ > 0$, it is unstable. If $f_+ > 0$ for all $x \leq D_\perp/2$, the structure not only is unstable but also is driven towards flux-line cutting in the plane $x = D_\perp/2$, where right-moving vortices (solid circles) meet left-moving vortices (open circles).

To examine the case of small perturbations, we make a Taylor's series expansion of $f_+(x)$ about the origin, which gives

$$f_+(x) = f_+(0) + xf_+'(0) + \frac{1}{2}x^2 f_+''(0) + \ldots \tag{2-25}$$

Since

$$f_+(0) = 0$$

by symmetry, we have

$$f_+(x) = xf_+'(0) + \frac{1}{2}x^2 f_+''(0) + \ldots \tag{2-26}$$

For small x,

$$f_+(x) \approx xf_+'(0) \tag{2-27}$$

When $f_+'(0) < 0$, Hooke's law applies and $f_+(x)$ is actually a restoring force which tends to pull the right-displaced vortices back to their initial positions (+). When $f_+'(0) > 0$, $f_+(x)$ drives the right-displaced vortices further away to the right. Therefore

$$f_+'(0) = 0 \tag{2-28}$$

gives the critical angle, $\Delta\alpha_c$, for the instability of the array to small perturbations.

For the case that $f_+(x) > 0$ in the region $0 < x < x_s (x_s < D_\perp/2)$, $f_+(x) < 0$ in the region $x_s < x < x_u (x_u < D_\perp/2)$, and $f_+(x) > 0$ in the region $x_u < x < D_\perp/2$, the structure is unstable at $x = 0$ to small perturbations and is driven to the position x_s where it is stable. Hence, the instability at $x = 0$ does not necessarily lead to flux-line cutting but does so only when $f_+(x) > 0$ for all $x < D_\perp/2$. The initial angle for flux-line cutting, $\Delta\alpha_{cm}$, for this particular case is then defined as the smallest angle for which $f_+(x) \geq 0$ for all $0 \leq x \leq D_\perp/2$. At this angle the region $x_s \leq x \leq x_u$ has shrunk to zero width such that $x_s = x_u = x_m$ and $f_+'(x_m) = f_+(x_m) = 0$. In this case, we define $\Delta\alpha_{co}$ as the angle which makes $f_+'(0) = 0$.

CHAPTER III. NUMERICAL CALCULATIONS

For the numerical calculations of $f_+(x)$ and $\bar{j}_{c\parallel}$ described in Chapter II, reduced (dimensionless) quantities denoted by tildes are used. The usual Ginzburg-Landau conventions[39] are employed in which length is measured in units of λ, magnetic field in units of $\sqrt{2}H_c = \kappa\phi_0/2\pi\lambda^2$, energy per unit volume in units of $H_c^2/4\pi$, force per unit length in units of $H_c^2\lambda/4\pi = \kappa^2\phi_0^2/32\pi^3\lambda^3$, and current density in units of $c\sqrt{2}H_c/4\pi\lambda$.

In reduced units, we have

$$\tilde{f}_+(\tilde{x}) = \sum_{n=-\infty}^{\infty} \tilde{f}_{+n}(\tilde{x})$$

$$= \sum_{|n|=1}^{\infty} \tilde{f}_{+n}(\tilde{x}) + \tilde{f}_{+0}(\tilde{x}) \qquad (3\text{-}1)$$

For $n \neq 0$,

$$\tilde{f}_{+n}(\tilde{x}) = [2\pi^2 r^3 A/(\kappa^2 \tilde{D}_{\parallel})]\cdot[\cos(n\Delta\alpha)\exp(-\tilde{X}_{nB}) - \exp(-\tilde{X}_{nB}\kappa\sqrt{2})]\cdot$$

$$(2\tilde{x} - n\tilde{D}_{\perp})/\tilde{X}_{nB} \qquad (3\text{-}2)$$

where

$$r = (1 - b)^{1/2}$$

and

$$\tilde{X}_{nB} = [r^2(n\tilde{D}_{\perp} - 2\tilde{x})^2 + \tilde{\xi}_v^2]^{1/2}$$

Here,

$$b = B_0/H_{c2} \qquad (3\text{-}3)$$

with

$$B_0 = \phi_0/D_{\perp}D_{\parallel}$$

For $n = 0$,

$$\tilde{f}_{+0}(\tilde{x}) = (16\pi r^4 A/\kappa^2) \sum_{m=1}^{\infty} [K_1(\tilde{S}_{mB}) - \kappa\sqrt{2}K_1(\tilde{S}_{mB}\kappa\sqrt{2})]\tilde{x}/\tilde{S}_{mB} \tag{3-4}$$

$$= \sum_{m=1}^{\infty} \tilde{f}^m_{+0}(\tilde{x}) \tag{3-5}$$

where

$$\tilde{f}^m_{+0}(x) = (16\pi r^4 A/\kappa^2)[K_1(\tilde{S}_{mB}) - \kappa\sqrt{2}K_1(\tilde{S}_{mB}\kappa\sqrt{2})]\tilde{x}/\tilde{S}_{mB} \tag{3-6}$$

and

$$\tilde{S}_{mB} = \{r^2[(2\tilde{x})^2 + (2m-1)^2\tilde{D}_{\|}^2] + \tilde{\xi}_v^2\}^{1/2}$$

For larger $|n|$ or m, the corresponding exponential or modified Bessel function terms drop off dramatically. The infinite series can be approximated by finite series as long as enough terms are kept. The maximum index for $|n|$ in the finite series, N, is obtained whenever

$$[2\pi^2 r^3 A/(\kappa^2\tilde{D}_{\|})]\exp(-\tilde{S}_{NB}) < 10^{-6} \sum_{|n|=1}^{N} \tilde{f}_{+n}(\tilde{x}) \tag{3-7}$$

and the maximum index for m, M, is obtained whenever

$$\tilde{f}^M_{+0}(\tilde{x}) < 10^{-6} \sum_{m=1}^{M} \tilde{f}^m_{+0}(\tilde{x}) \tag{3-8}$$

To solve for the root, the critical angle $\Delta\alpha_c$, of the nonlinear equation

$$\tilde{f}'_+(0, \Delta\alpha) = 0 \tag{3-9}$$

where $\Delta\alpha$ is a parameter of $\tilde{f}'_+$, we use Newton's method.[40] In this method, we start with an initial trial value, $\Delta\alpha_0$, then calculate $\tilde{f}'_+(0, \Delta\alpha_0)$ and $d\tilde{f}'_+(0, \Delta\alpha)/d(\Delta\alpha)$ evaluated at $\Delta\alpha_0$. Let

$$\tilde{g}(\Delta\alpha) = d\tilde{f}'_+(0, \Delta\alpha)/d(\Delta\alpha) \tag{3-10}$$

The next trial value for $\Delta\alpha_c$ is found by the formula

$$\Delta\alpha_1 = \Delta\alpha_0 - \tilde{f}'_+(0, \Delta\alpha_0)/\tilde{g}(\Delta\alpha_0) \tag{3-11}$$

The procedure is then repeated to generate a sequence $\Delta\alpha_2$, $\Delta\alpha_3$, ... which converges quadratically to $\Delta\alpha_c$. The general formula for the k-th iteration is given by

$$\Delta\alpha_{k+1} = \Delta\alpha_k - \tilde{f}'_+(0, \Delta\alpha_k)/\tilde{g}(\Delta\alpha_k) \tag{3-12}$$

In the computer program, we use two criteria for stopping the iteration. That is, with a tolerance

$$\varepsilon = 10^{-6}$$

we require that

$$|\tilde{f}_+(0, \Delta\alpha_n)| < \varepsilon \tag{3-13}$$

and

$$|\tilde{f}'_+(0, \Delta\alpha_n)/\tilde{g}(\Delta\alpha_n)| < 10^{-4}\,\varepsilon \tag{3-14}$$

be satisfied to give an approximate root, $\Delta\alpha_n$, for $\Delta\alpha_c$.

From Eqs. (3-1), (3-2), and (3-5), it follows that

$$\begin{aligned}\tilde{f}'_+(0, \Delta\alpha_k) = {} & (16\pi A/\kappa^2) \sum_{m=0}^{\infty} K_1(\tilde{S}_{mB0})/\tilde{S}_{mB0} \\ & - (16\pi A/\kappa^2) \sum_{m=0}^{\infty} \kappa\sqrt{2}K_1(\tilde{S}_{mB0}\sqrt{2}\kappa)/\tilde{S}_{mB0} \\ & + [8\pi^2 A/(\kappa^2\tilde{D}_{\|})] \sum_{n=1}^{\infty} \exp(-\tilde{X}_{nB0}\kappa\sqrt{2})[(rn\tilde{D}_{\perp})^2\tilde{X}_{nB0}\kappa\sqrt{2} - \tilde{\xi}_v^2]/ \\ & \tilde{X}_{nB0}^3 \\ & - [8\pi^2 A/(\kappa^2\tilde{D}_{\|})] \sum_{n=1}^{\infty} \cos(n\Delta\alpha_k)\exp(-\tilde{X}_{nB0})[(rn\tilde{D}_{\perp})^2\tilde{X}_{nB0} \\ & - \tilde{\xi}_v^2]/\tilde{X}_{nB0}^3 \end{aligned} \tag{3-15}$$

$$= S_1 + S_2 + S_3 + S_4$$

where $S_1, \ldots, S_4$ represent the four corresponding infinite series on the right-hand side and

$$\tilde{S}_{mBO} = \{[r(2m - 1)\tilde{D}_{\parallel}]^2 + \tilde{\xi}_v^2\}^{1/2}$$

$$\tilde{X}_{nBO} = [(4n\tilde{D}_{\perp})^2 + \tilde{\xi}_v^2]^{1/2}$$

$\tilde{g}(\Delta\alpha_k)$ is found to be

$$\tilde{g}(\Delta\alpha_k) = [8\pi^2 A/(\kappa^2\tilde{D}_{\parallel})] \sum_{n=1}^{\infty} n[(rn\tilde{D}_{\perp})^2\tilde{X}_{nBO} - \tilde{\xi}_v^2]\sin(n\Delta\alpha_k)\exp(-\tilde{X}_{nBO})/\tilde{X}_{nBO}^3$$

$$= S_5 \qquad (3\text{-}16)$$

The infinite series are again approximated by finite series for the evaluation of $S_1, \ldots, S_5$. We require that the last term in each finite series ignoring cosine and sine factors be less than

$$10^{-6} \times (\text{finite series})_i$$

where $i = 1, \ldots, 5$. However, a second cutoff criterion for each series is employed in the limit that $\tilde{\xi}_v \to 0$. Let ΔS_1 represent the sum of the terms to be neglected in S_1, i.e.,

$$\Delta S_1 = (16\pi A/\kappa^2) \sum_{m=M_1+1}^{\infty} K_1(\tilde{S}_{mBO})/\tilde{S}_{mBO} \qquad (3\text{-}17)$$

where M_1 is the maximum index in the finite series approximation to S_1. The upper limit of Δs_1 is found to be (Appendix A)

$$[4\pi A/(r^2 M_1 \kappa^2 \tilde{D}_{\parallel}^2)]K_0(2rM_1\tilde{D}_{\parallel}) \qquad (3\text{-}18)$$

The second criterion requires that Eq. (3-18) be less than 10^{-6} times the approximate finite series. A similar cutoff procedure is used for S_2. For S_3, S_4, and S_5, the upper limits for each series, called LS_3, LS_4, and LS_5 can be calculated (Appendix B) to be

$$LS_3 = [8\pi^2 A/(\kappa^2 \tilde{D}_{\parallel})]\kappa\sqrt{2}\, \exp(-r\kappa\sqrt{2}\tilde{D}_{\perp}) \tag{3-19}$$

$$LS_4 = -[8\pi^2 A/(\kappa^2 \tilde{D}_{\parallel})][\exp(r\tilde{D}_{\perp})\cos \Delta\alpha_k - 1]/$$

$$\{[\exp(r\tilde{D}_{\perp})\cos \Delta\alpha_k - 1]^2 + [\exp(r\tilde{D}_{\perp})\sin \Delta\alpha_k]^2\} \tag{3-20}$$

and

$$LS_5 = [8\pi^2 A/(\kappa^2 \tilde{D}_{\parallel})][\exp(2r\tilde{D}_{\perp}) - 1]\exp(r\tilde{D}_{\perp})\sin \Delta\alpha_k/$$

$$\{[\exp(r\tilde{D}_{\perp})\cos \Delta\alpha_k - 1]^2 + [\exp(r\tilde{D}_{\perp})\sin \Delta\alpha_k]^2\} \tag{3-21}$$

provided that $\tilde{\xi}_v \to 0$. The second cutoff criterion for each series then requires that the last term ignoring cosine and sine factors in each finite series approximation be less than

$$10^{-6} \times |LS_i|$$

where i = 3, 4, and 5.

CHAPTER IV. RESULTS

The forces per unit length of vortex in reduced units expected on a right-displaced vortex are plotted for $\tilde{D}_\perp < 0.62$, $\tilde{D}_\perp = 0.62$, and $\tilde{D}_\perp > 0.62$ in Figures 5, 6, and 7, respectively, for $\kappa = 10$ and $D_\parallel / D_\perp = \sqrt{3}$. The angles selected are indicated by points a - k shown in Figure 8.

In Figure 5, for the angle $\Delta\alpha$ corresponding to case a, the force $\tilde{f}_+$ is always positive and increasing with displacement. From the instability analysis described in Chapter II vortices are unstable at $x = 0$ and are driven to undergo flux-line cutting in the plane $x = D_\perp/2$. For the angle $\Delta\alpha$ corresponding to case b, the slope of the force at $x = 0$ is zero. This determines the critical angle, $\Delta\alpha_c$, for that particular $D_\perp$ value. For case c, $\Delta\alpha < \Delta\alpha_c$, the force $\tilde{f}_+$ is negative near the origin. This gives rise to a restoring force for small perturbations to stabilize the perturbed right-displaced vortices. Therefore flux-line cutting does not occur for case c for small perturbations.

In Figure 6, for case e the curve is rather flat over a certain range of displacements and then goes up. For this reason the corresponding $\Delta\alpha$ is the critical angle for $\tilde{D}_\perp = 0.62$. For case d, $\Delta\alpha > \Delta\alpha_c$ and for case f, $\Delta\alpha < \Delta\alpha_c$, which correspond respectively to unstable and stable vortices for small perturbations. The forces are weaker than in Figure 5.

In Figure 7, five curves are shown in which curves for cases g, j, and k correspond to cases d, e, and f, respectively, in Figure 6. For case j, the angle $\Delta\alpha$ corresponds to $\Delta\alpha_{co}$, when $\tilde{f}_+'(0) = 0$. For case i, initially unstable vortices at $x = 0$ become stable at $x = 0.195\ D_\perp$ where the curve intersects the $\tilde{f}_+ = 0$ line. For case k, the slope of the force

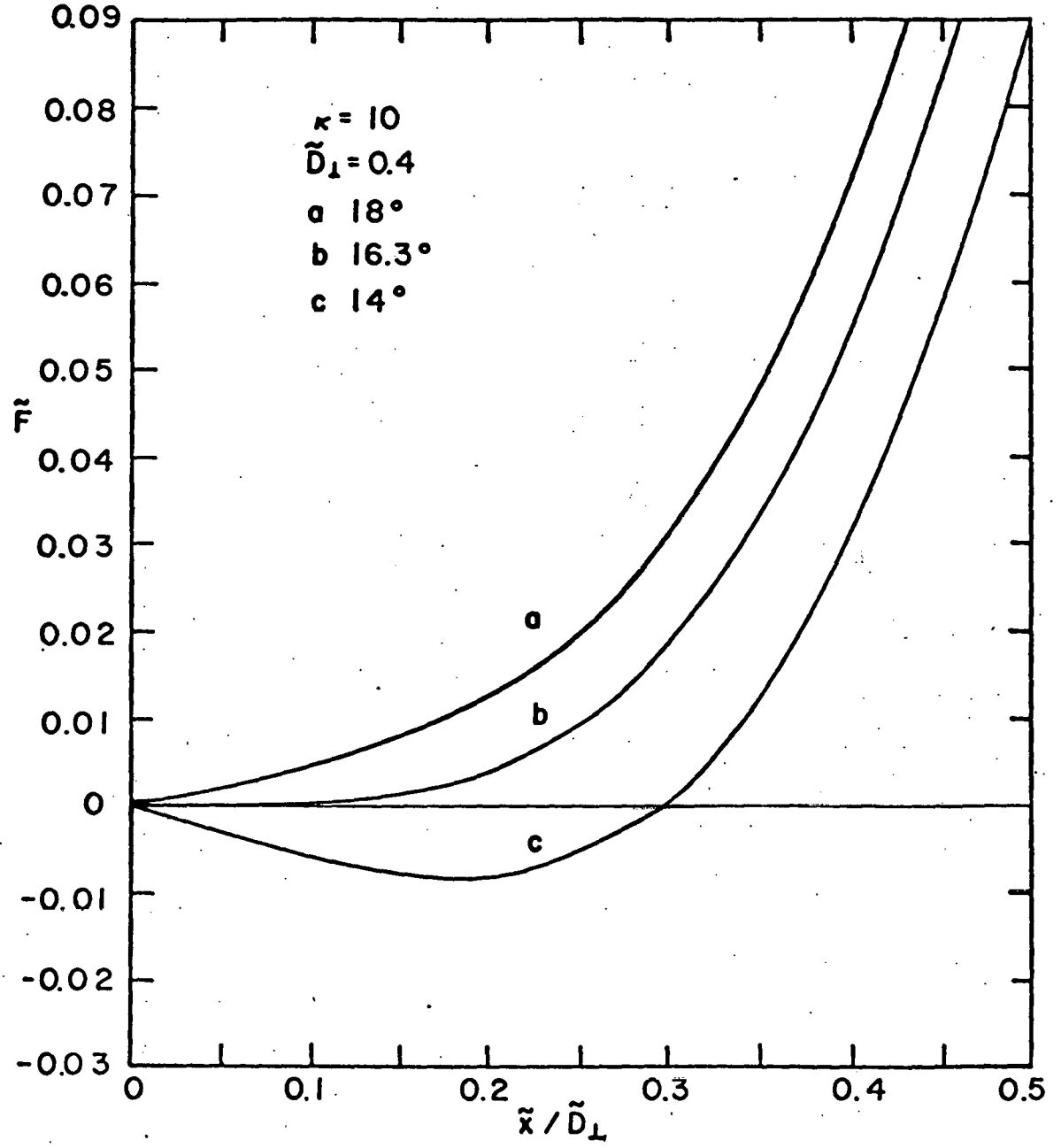

Figure 5. Reduced force $\tilde{F}$ (or $\tilde{f}_+$ as in the text) vs. $\tilde{x}$ for the angles $\Delta\alpha$ = 18°, 16.3°, and 14° at points a, b, and c of Figure 8; κ = 10, $\tilde{D}_\perp$ = 0.4, and $D_\parallel / D_\perp = \sqrt{3}$.

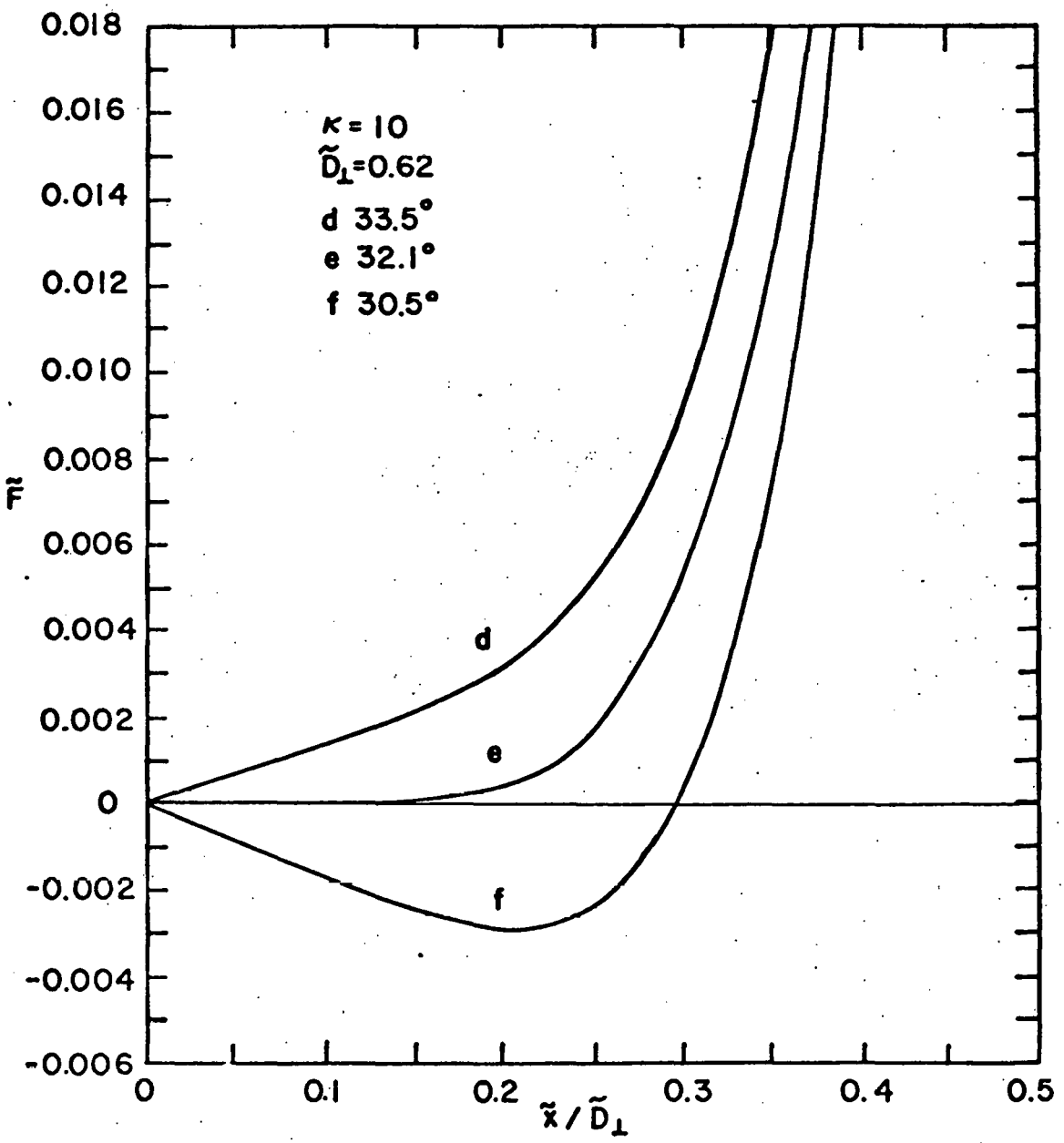

Figure 6. Reduced force $\tilde{F}$ vs. $\tilde{x}$ for the angles $\Delta\alpha$ = 33.5°, 32.1°, and 30.5° at points d, e, and f of Figure 8; κ = 10, $\tilde{D}_\perp$ = 0.62, and $D_\parallel / D_\perp = \sqrt{3}$.

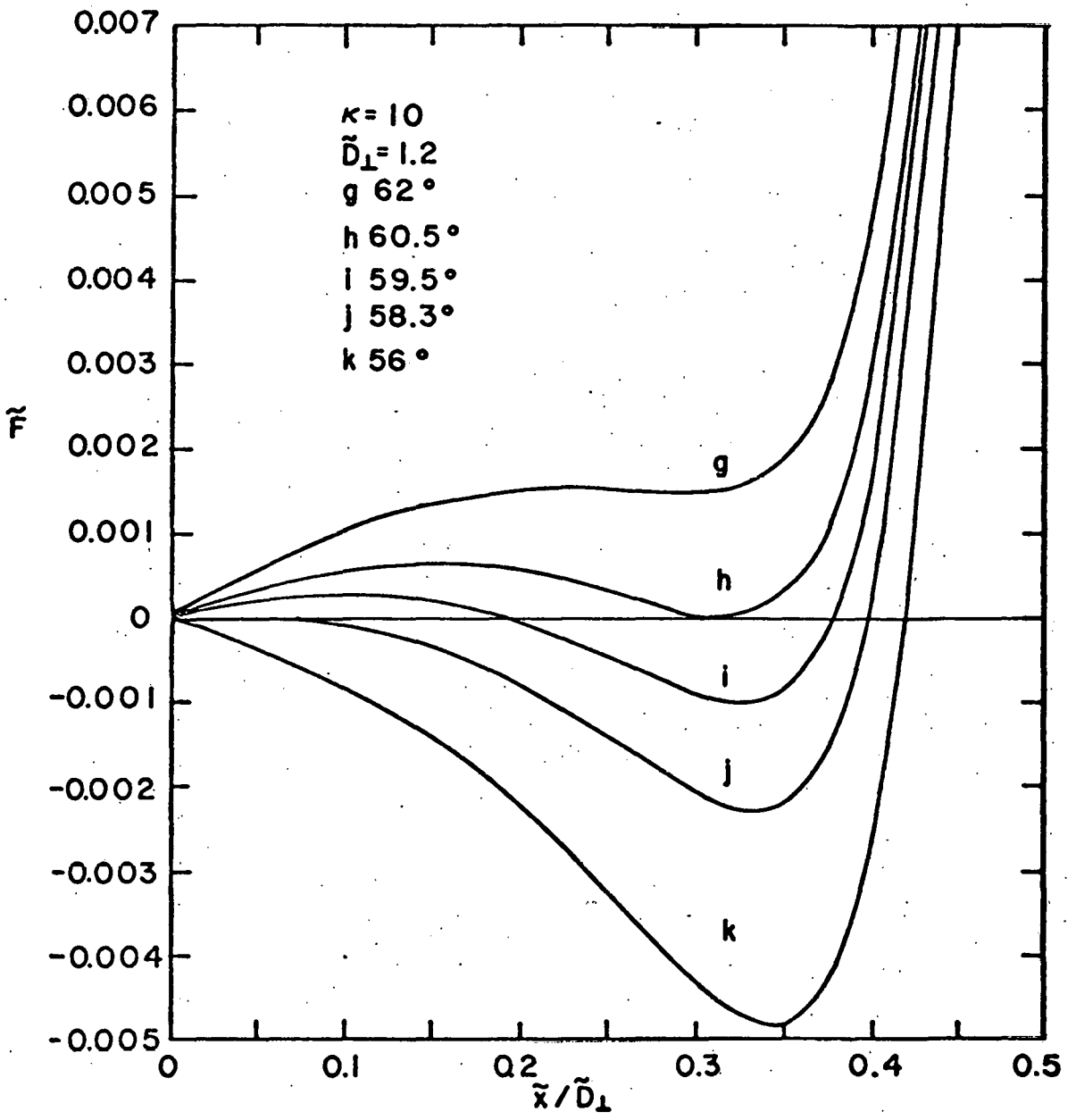

Figure 7. Reduced force $\tilde{F}$ vs. $\tilde{x}$ for the angles $\Delta\alpha$ = 62°, 60.5°, 59.5°, 58.3°, and 56° at points g, h, i, j, and k of Figure 8; κ = 10, $\tilde{D}_\perp$ = 1.2, and $D_\parallel/D_\perp = \sqrt{3}$.

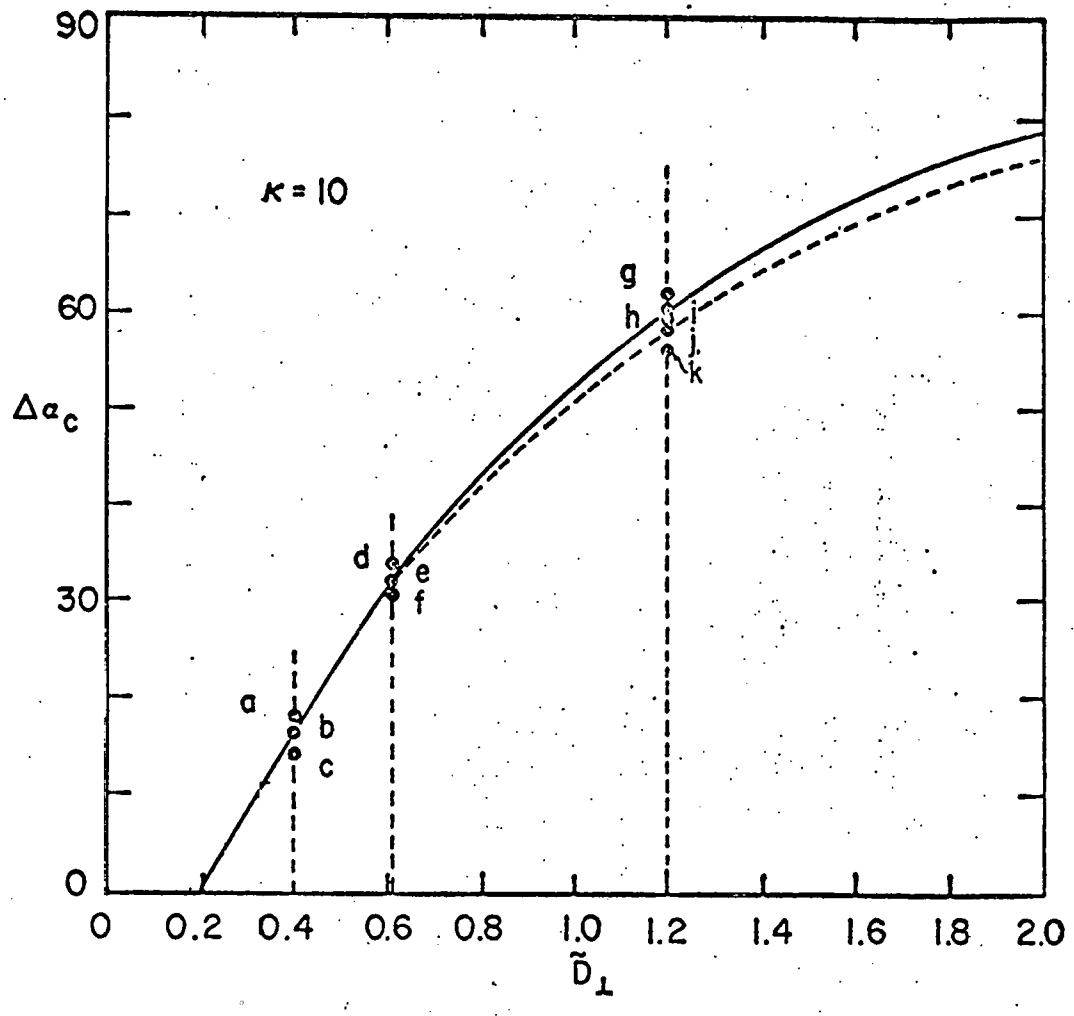

Figure 8. Critical angle difference $\Delta\alpha_c$ vs. $\tilde{D}_\perp$ for $\kappa = 10$ and $D_\parallel / D_\perp = \sqrt{3}$. The meaning of the short-dashed and solid curves is explained in the text. The behavior of $\tilde{f}_+(x)$ vs. $\tilde{x}$ for the angles at points a - k is shown in Figures 5-7.

$\tilde{f}_+$ is positive at x = 0 while it is zero at x = 0.32 $D_\perp$, where $\tilde{f}_+$ is also zero. This determines $\Delta\alpha_{cm}$, the critical angle for flux-line cutting. For $\Delta\alpha > \Delta\alpha_{cm}$, as in case g, $\tilde{f}_+ > 0$ for all $0 < x < D_\perp/2$ and any instability is driven towards flux-line cutting.

Critical angles (in degrees) vs. $\tilde{D}_\perp$ for $\kappa = 10$ and $D_\parallel / D_\perp = \sqrt{3}$ are plotted in Figure 8 with $\Delta\alpha_{co}$ indicated by a dashed curve. Flux-line cutting occurs for those angles above the solid curve. For angles below the solid ($\tilde{D}_\perp \leq 0.62$) or dashed curves ($\tilde{D}_\perp > 0.62$), vortices are stable at x = 0 to small perturbations. For angles between the solid and dashed curves, vortices are unstable at x = 0 but stable at some displacement less than $D_\perp/2$ such that flux-line cutting does not necessarily occur. The points indicate the angles appearing in Figures 5, 6, and 7. In the following figures for $\Delta\alpha_c$ vs. $\tilde{D}_\perp$ or b, $\tilde{k}_c$ vs. b, and $\tilde{k}_c\tilde{\lambda}_B$ vs. b, the short dashed lines have the same meaning as in Figure 8 and $D_\parallel / D_\perp = \sqrt{3}$ unless indicated in the figures.

Critical angles vs. $\tilde{D}_\perp$ for different κ values are plotted in Figure 9. Along the curves, $f_+'(0) = 0$. Here the $\Delta\alpha_{cm}$ curves are neglected. It can be seen for low κ material that flux-line cutting is more probable and that the critical angle is depressed considerably. Stable vortex arrays are associated with larger intervortex spacings and smaller interplanar angles.

The results of Figure 9 are replotted in Figures 10 and 11, which show the dependence of $\Delta\alpha_c$ on b for different κ values, where $b = B_0/B_{c2}$ with $B_0 = \phi_0/D_\perp D_\parallel$. It is seen that $\Delta\alpha_c$ is a monotonically decreasing

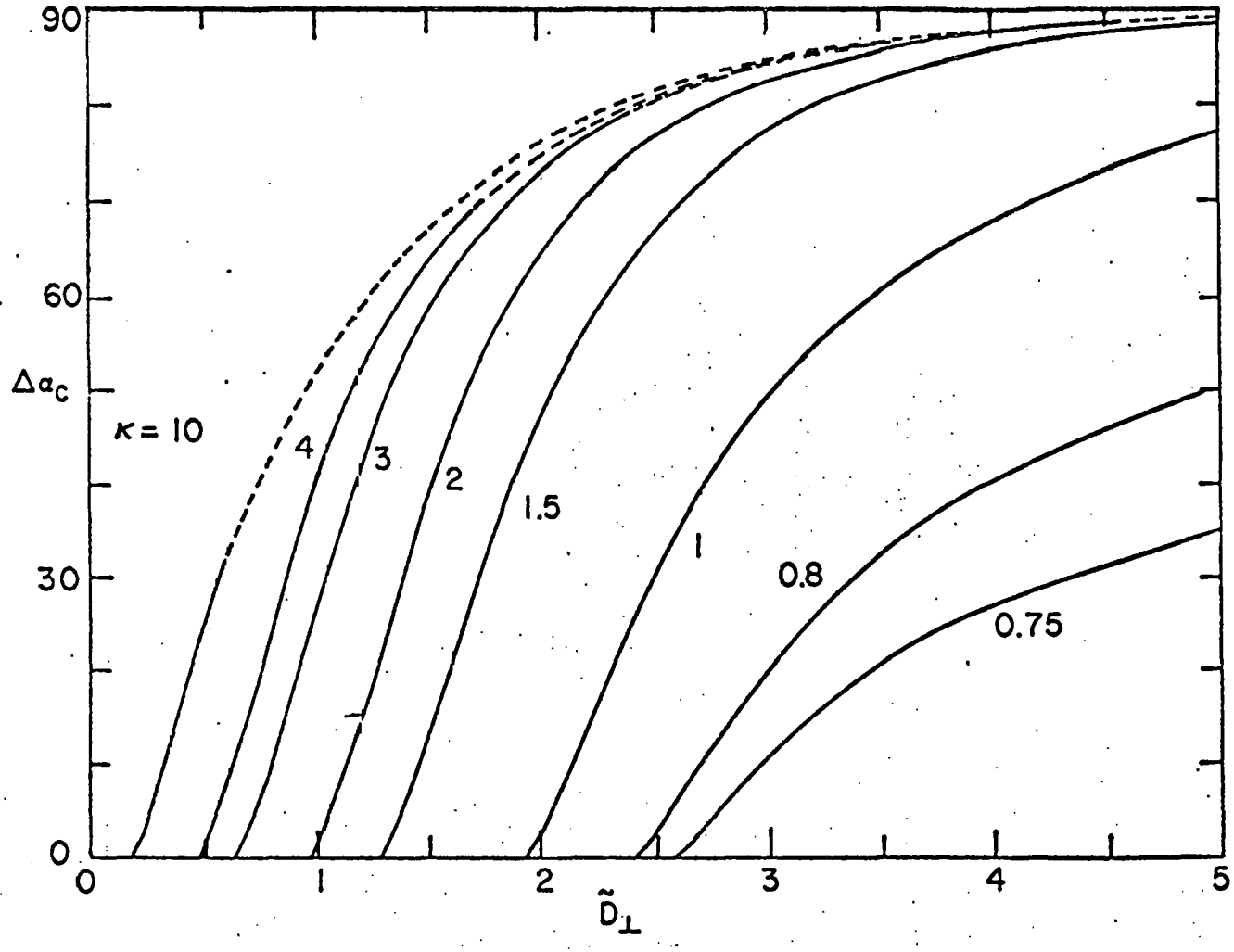

Figure 9. $\Delta\alpha_c$ vs. $\tilde{D}_\perp$ for $D_\parallel / D_\perp = \sqrt{3}$ and various values of κ. The short dashes are described in the text.

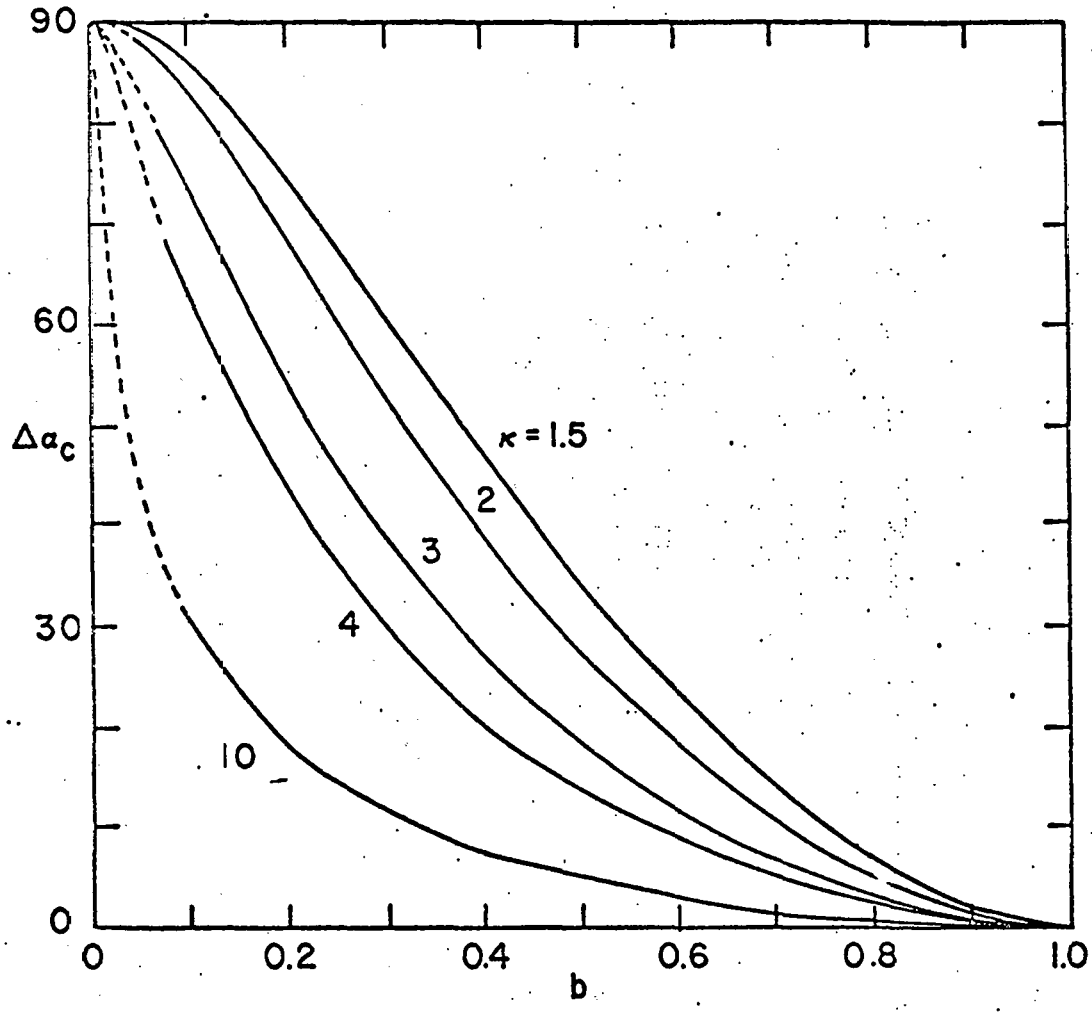

Figure 10. $\Delta\alpha_c$ vs. $b = B_0/B_{c2}$, where $B_0 = \phi_0/D_{\parallel} D_{\perp}$ and $B_{c2} = \phi_0/2\pi\xi^2$, for $D_{\parallel}/D_{\perp} = \sqrt{3}$ and κ = 1.5, 2, 3, 4, and 10.

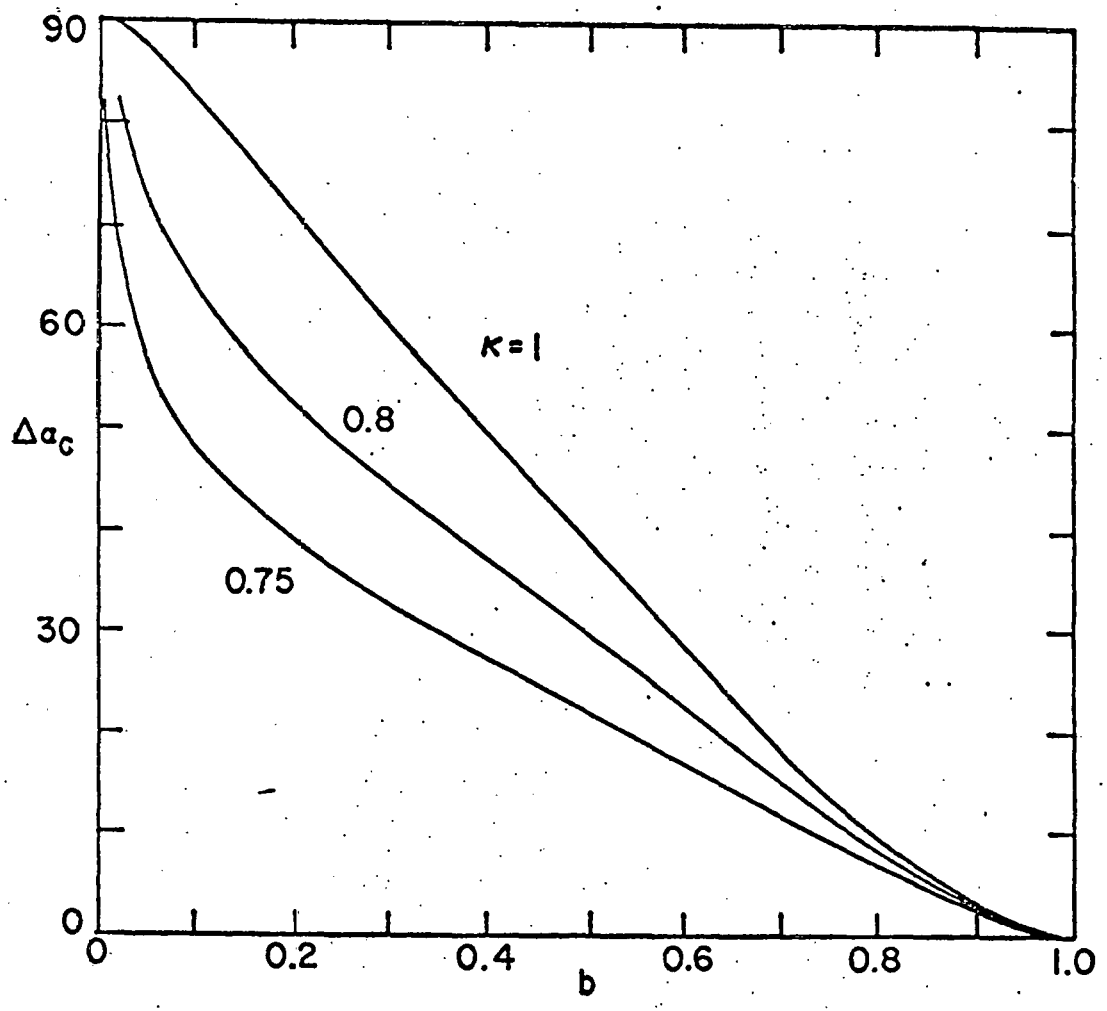

Figure 11. $\Delta\alpha_c$ vs. b for $D_{\parallel}/D_{\perp} = \sqrt{3}$ and κ = 0.75, 0.8, and 1.

function of b. For a fixed b, when $\kappa \geq 1.5$, $\Delta\alpha_c$ is higher for lower κ materials, but for $\kappa \leq 1$ the opposite behavior is observed.

For $\Delta\alpha = 0$, three vortex structures with different ratios of $D_{\parallel}/D_{\perp}$ are plotted in Figure 12. The ratio $D_{\parallel}/D_{\perp} = \sqrt{3}$ as shown in Figure 12a is that found for the steady-state flux-line cutting model of Clem[27] by requiring minimum entropy production. The case $D_{\parallel}/D_{\perp} = 2\sqrt{3}$ corresponds to a triangular lattice with a nearest-neighbor vector perpendicular to the vortex planes as shown in Figure 12b. Shown in Figure 12c is the case $D_{\parallel}/D_{\perp} = 2\sqrt{3}$ corresponding to a triangular lattice with a nearest neighbor vector parallel to the vortex planes.

Figure 13 exhibits the critical angles for different ratios of $D_{\parallel}/D_{\perp}$ as functions of b with two different κ values. The curves show that $\Delta\alpha_c$ depends primarily upon b or κ rather than the ratios of $D_{\parallel}/D_{\perp}$.

In Figure 14, the reduced critical angle gradient, $\tilde{k}_c$, is plotted as a function of b for each κ value, where

$$\tilde{k}_c = \Delta\alpha_c/\tilde{D}_{\perp} \tag{4-1}$$

This quantity also gives the critical value of the reduced wave number $\tilde{k}$ in the equation for the macroscopic flux density $\vec{B}(x)$ given by Eq. (2-18).

Shown in Figure 15 is $\tilde{k}_c\tilde{\lambda}_B$ vs. b for different κ values. Eq. (2-18) gives the magnitude of flux density as

$$B(x) = B_0/[1 + (\tilde{k}\tilde{\lambda}_B)^2] \tag{4-2}$$

Here, B_0 is independent of $\tilde{k}$. Thus B(x) is reduced by a factor $[1 + (\tilde{k}\tilde{\lambda}_B)^2]$ from the constant value of B_0. The bigger $\tilde{k}\tilde{\lambda}_B$ is the more B(x) is reduced. The peaks of the curves shift to higher b for decreasing κ values.

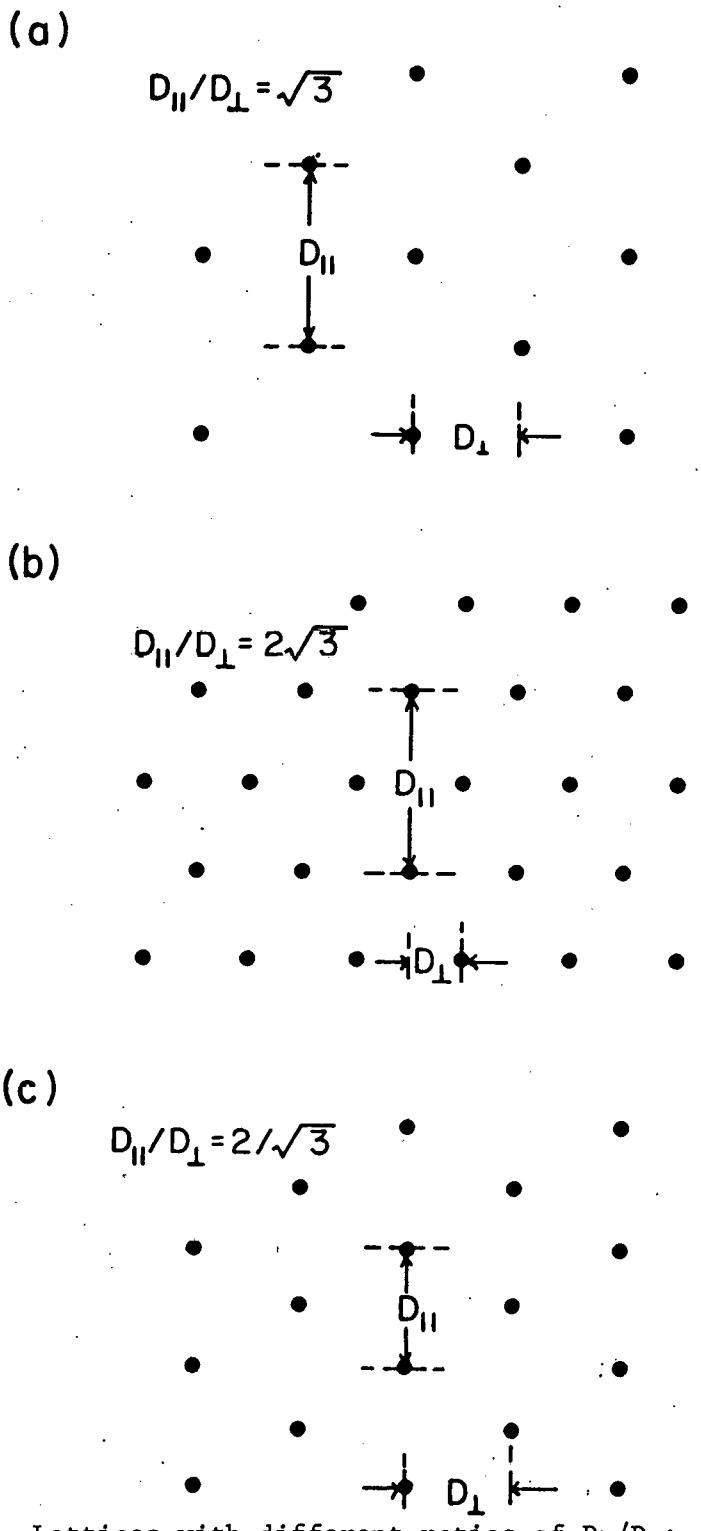

Figure 12. Lattices with different ratios of $D_{\parallel}/D_{\perp}$: (a) $\sqrt{3}$, (b) $2\sqrt{3}$, and (c) $2/\sqrt{3}$.

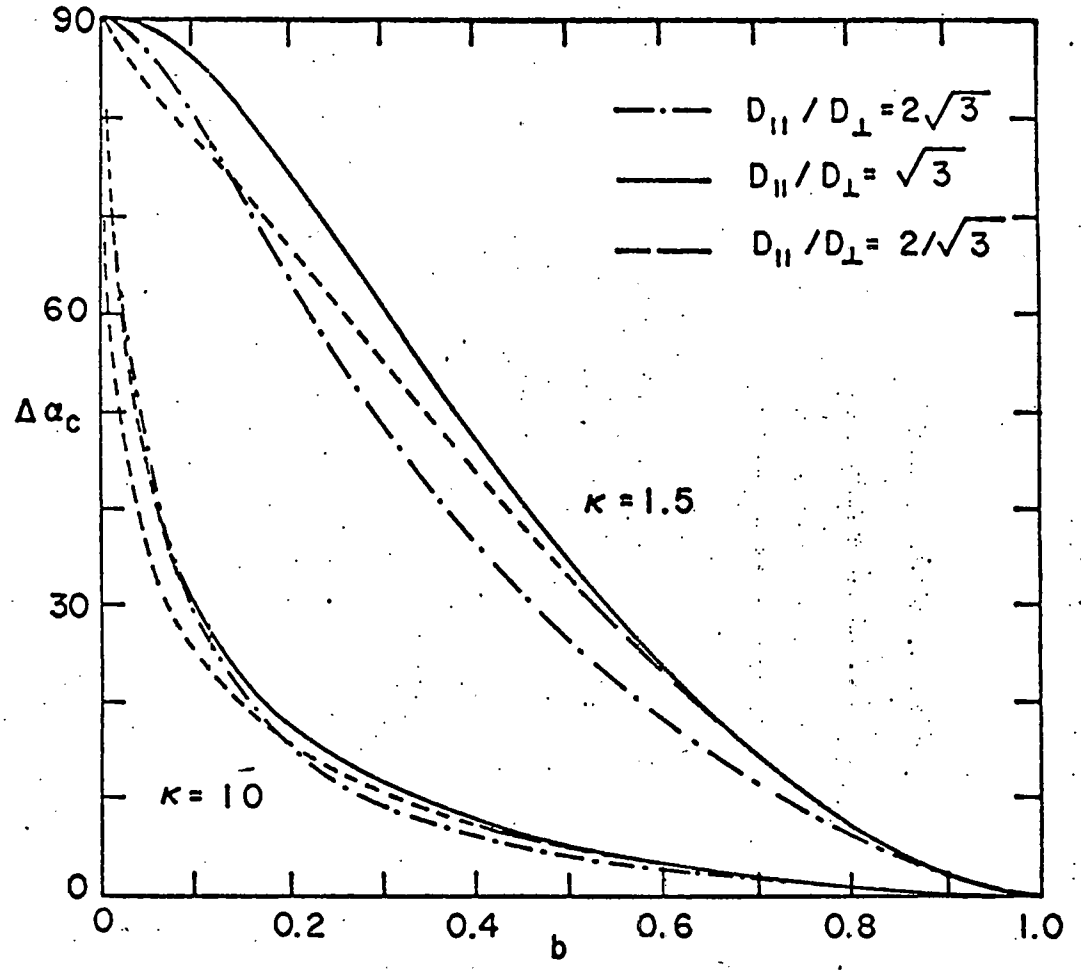

Figure 13. $\Delta\alpha_c$ vs. b for $D_{\parallel} / D_{\perp} = 2\sqrt{3}$, $\sqrt{3}$ and $2/\sqrt{3}$ and $\kappa = 1.5$.

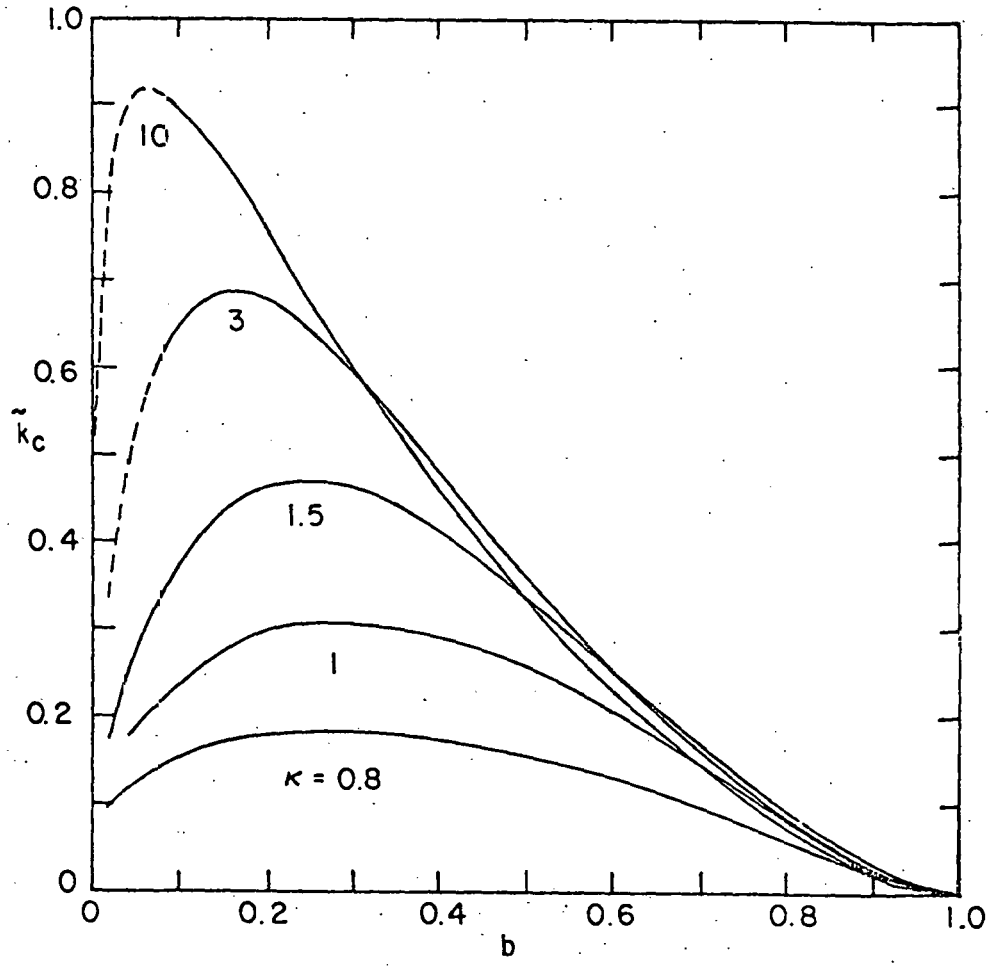

Figure 14. Reduced critical angle gradient $\tilde{k}_c = \Delta\alpha_c/\tilde{D}_\perp$ vs. b for $D_\parallel/D_\perp = \sqrt{3}$ and κ = 0.8, 1, 1.5, 3, and 10.

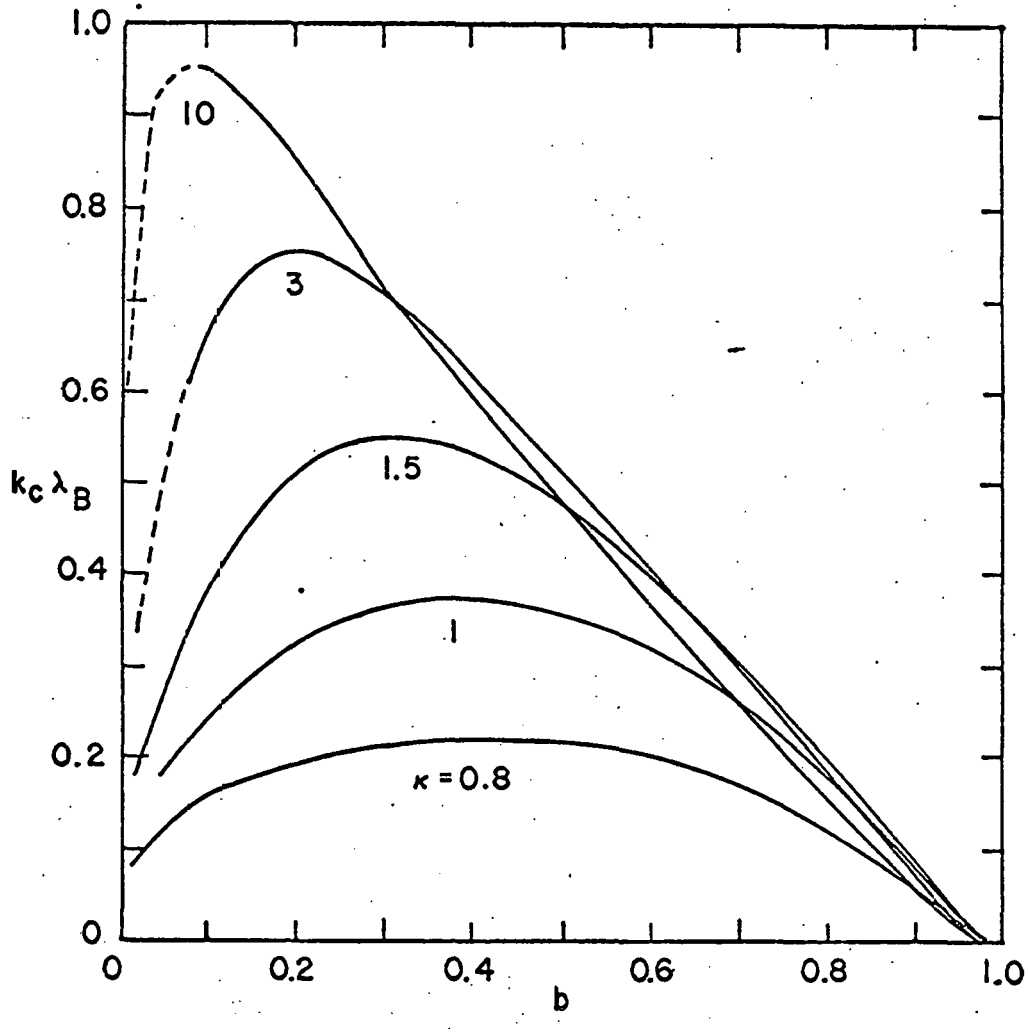

Figure 15. $\tilde{k}_c\tilde{\lambda}_B$ vs. b where $\tilde{\lambda}_B$ is the reduced field-dependent penetration depth, for $D_{\parallel}/D_{\perp} = \sqrt{3}$ and κ = 0.8, 1, 1.5, 3, and 10.

The reduced longitudinal critical current density $\tilde{j}_{c\parallel}$ vs. b determined by Eq. (2-19) is plotted in Figure 16. There is a maximum value for each parameter κ. These peaks tend to shift to the right for lower κ. The critical current density decreases rapidly as κ decreases, which implies that flux-line cutting occurs more easily in low κ materials.

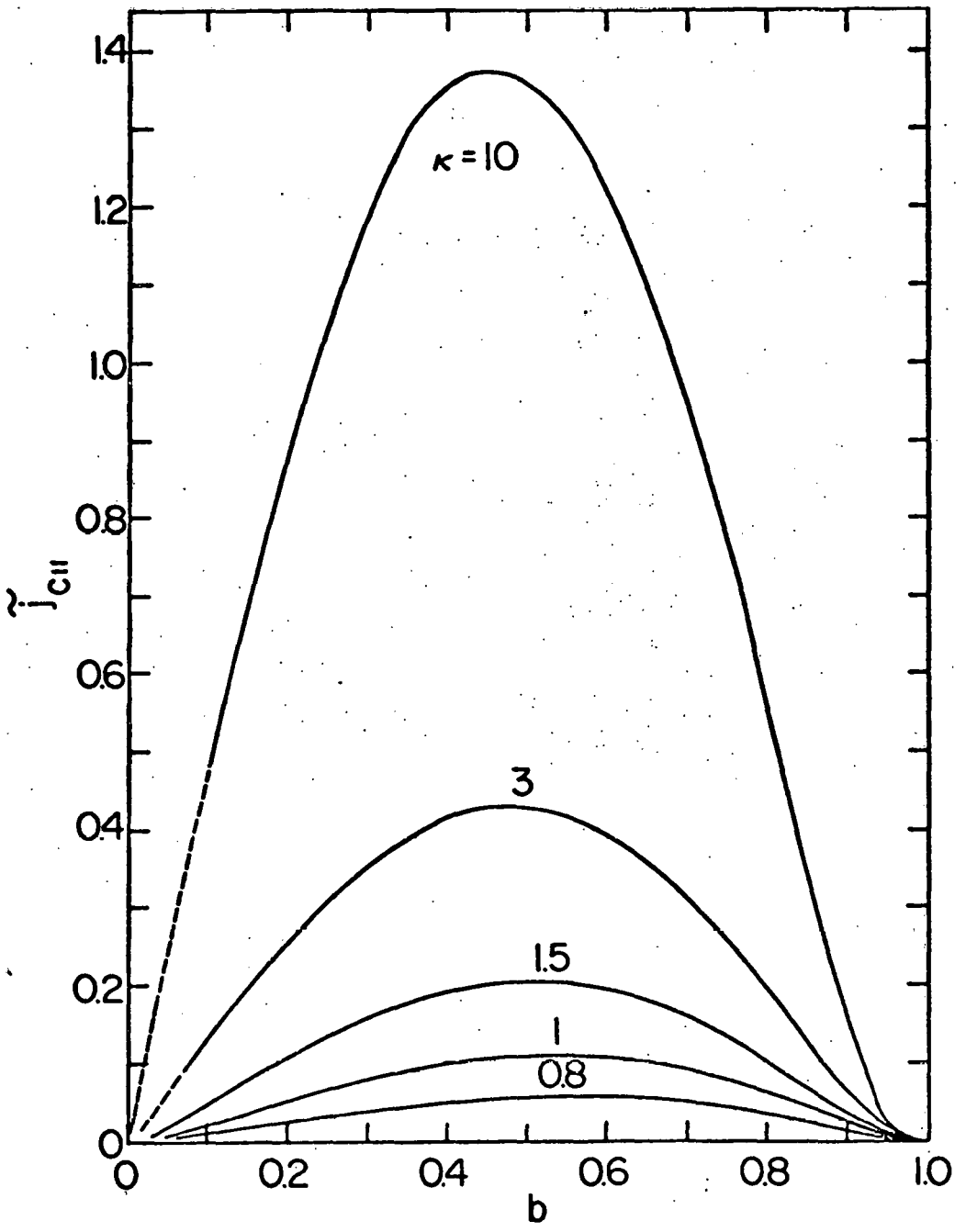

Figure 16. Reduced parallel critical current density $\tilde{j}_{c\parallel}$ vs. b for $D_{\parallel}/D_{\perp} = \sqrt{3}$ and κ = 0.8, 1, 1.5, 3, and 10.

CHAPTER V. DISCUSSION AND CONCLUSIONS

In this thesis, the stability of the vortex array in a slab geometry is analyzed. Numerical calculations of the force exerted on a vortex in a perturbed array exhibit the existence of a threshold for flux-line cutting. For angles exceeding the critical value, the array is driven towards flux-line cutting for small perturbations. The critical angle gradient, k_c, can be employed to express the threshold for flux-line cutting. It is of interest to compare our k_c with LeBlanc and co-workers' empirical expression[28-31] for the critical angle gradient. Their empirical expression is

$$\frac{d\phi}{dx} = \pm \frac{k(T)F_p(B)}{B^2} \cos^2\phi \tag{5-1}$$

where ϕ is the angle that vortices make with the z-axis, B is the magnetic induction, k(T) is a adjustable temperature dependent parameter and $F_p(B)$ is the volume pinning force function. $F_p(B)$ has been found empirically as

$$F_p(B) = \alpha(T)B^n[1 - (B/B_{c2})^{\ell}]^m \tag{5-2}$$

where α is a temperature dependent parameter, n, ℓ, and m are real numbers, usually taken to be small positive integers or half integers.

In Figure 14, our k_c vanishes as B approaches B_{c2}. This is in qualitative agreement with Eq. (5-1), in which $F_p(B)$ vanishes as seen from Eq. (5-2). However, by Eqs. (5-1) and (5-2), the empirical $d\phi/dx$ vanishes for ideal, pinning-free superconductors, in contrast to the predicted exist-

ence of a nonzero critical angle gradient under the pinning-free assumption of our model.

Timms and Walmsley[16] have stated that pinning sites of appropriate size can reduce the cutting "activation energy" to a dramatic extent. This favors the occurrence of flux-line cutting. Thus the critical angle gradient in irreversible materials is expected to be smaller than in homogeneous materials. But by Eq. (5-1), the opposite result is predicted. Further theoretical and experimental work is needed to clarify how pinning affects a vortex array on the verge of flux-line cutting.

Close to b = 1, where the self-field of the current is negligible, the longitudinal critical current density or the depairing critical current density of a bulk type-II superconductor in reduced units is calculated via Ginzburg-Landau theory to be[6,9,10,11]

$$\tilde{j}_{c\parallel} = 0.385(1 - b)^{3/2} / \beta_A(1 - 1/2\kappa^2) \qquad (5\text{-}3)$$

where $\beta_A = 1.1596$ for the equilaterial triangular lattice.

The values of $\tilde{j}_{c\parallel}$ given by Eq. (5-3) are somewhat less than our calculated $\tilde{j}_{c\parallel}$ for $\kappa \geq 1$. In a theoretical calculation which would take into account the depairing effect, the calculated k_c and $\Delta\alpha_c$ should be smaller than those of the present theory.

From considerations of fluxoid conservation as discussed by Clem[27], we see that, after vortices from the planes x = 0 and x = D undergo flux-line cutting and straightening, the resulting vortices make an angle $\Delta\alpha/2$ relative to the z axis and have new values of the intervortex spacing $D'_{\parallel}$ and the reduced vortex density b'. They are related to the initial $D_{\parallel}$ and b by

$$D'_{\parallel} / D_{\parallel} = \sec(\Delta\alpha/2) > 1 \qquad (5\text{-}4)$$

and

$$b'/b = \cos(\Delta\alpha/2) < 1$$

By symmetry, other resulting vortices are in the planes at $x = \pm D_{\perp}/2$, $\pm 3D_{\perp}/2$, $\pm 5D_{\perp}/2$, ... with the corresponding angles $\alpha = \pm\Delta\alpha/2$, $\pm 3\Delta\alpha/2$, $\pm 5\Delta\alpha/2$, ... Because the angle between the vortices in adjacent planes is again $\Delta\alpha$ and the interplanar spacing is still $D_{\perp}$, the resulting structure is very similar to the original one, except that the reduced vortex density b' is smaller than before. From Figures 10, 11, and 13, we see that $\Delta\alpha_c$ is a monotonically decreasing function of b. Therefore, the resulting structure is closer to stability, with a higher critical angle for the next flux-line-cutting event. In fact, if $\Delta\alpha_c(b') > \Delta\alpha > \Delta\alpha(b)$, the new structure is stable. If not, flux-line cutting occurs again and again, finally producing a stable structure with $b^{(n)} = b \cos^n(\Delta\alpha/2)$, for which $\Delta\alpha_c(b^{(n)}) > \Delta\alpha > \Delta\alpha_c(b)$ after a total of n flux-line-cutting events. Because the density of vortices in the final, stable structure is smaller than that in the initial structure, the stored energy in the vortex array is also less. The energy difference is converted into heat via the viscous motion of the vortices through the metal lattice. This shows that flux-line cutting is an irreversible process.

In this work, we have considered only one perturbation as sketched in Figure 4, which preserves the straightness of all vortices in each plane. For instabilities involving the bending or curling of vortices,[8,23] it is possible that smaller critical values of $\Delta\alpha_c$ and k_c occur, as in the case

when the depairing effect is taken into account. Therefore, the values of $\Delta\alpha_c$ and k_c in this thesis represent upper limits to the true values.

Experiments in slab geometry are often difficult to analyze because of edge and demagnetization effects. Thus many related experiments have been performed not in slab geometry but in cylindrical geometry. It would be desirable to extend the present approach to the latter. The present results are expected to be valid even in cylindrical geometry provided that k_c^{-1} is small by comparison with the radius of curvature of a helical vortex. However, the concept of a critical angle gradient in slab geometry probably should be replaced by that of a critical pitch gradient in cylindrical geometry. The reason for this is that two helical vortices of the same pitch, when brought close to each other at the same radial coordinate, are locally parallel to each other and therefore cannot reduce their energy via flux-line cutting.

REFERENCES

1. S. T. Sekula, R. W. Boom, and C. J. Bergeron, Appl. Phys. Lett. 2, 102 (1963).

2. C. J. Bergeron, Appl. Phys. Lett. 3, 63 (1963).

3. J. W. Heaton and A. C. Rose-Innes, Phys. Lett. 9, 112 (1964).

4. M. A. R. LeBlanc, B. C. Belanger, and R. M. Fielding, Phys. Rev. Lett. 14, 704 (1965).

5. M. A. R. LeBlanc, Phys. Rev. 143, 220 (1966).

6. R. G. Boyd, Phys. Rev. 145, 255 (1966).

7. H. London and D. G. Walmsley, in Proceedings 11th Int. Conf. Low Temp. Phys. (St. Andrews, 1968), p. 879.

8. M. Sugahara, Appl. Phys. 41, 3668 (1970).

9. V. R. Karasik and V. G. Vereshchagin, Sov. Phys.-JETP 32, 20 (1971).

10. F. F. Ternovskii, Sov. Phys.-JETP 33, 969 (1971).

11. R. O. Zaitsev, Sov. Phys.-JETP 34, 864 (1972).

12. D. G. Walmsley, J. Phys. F 2, 510 (1972).

13. A. M. Campbell and J. E. Evetts, Adv. Phys. 21, 199 (1972).

14. D. G. Walmsley and W. E. Timms, J. Phys. F 3, L203 (1973).

15. J. F. Nicholson and P. T. Sikora, J. Low Temp. Phys. 17, 275 (1974).

16. W. E. Timms and D. G. Walmsley, J. Phys. F 5, 287 (1975).

17. K. Yamafuji, T. Kawashima, and H. Ichikawa, J. Phys. Soc. Japan 39, 581 (1975).

18. J. R. Clem, Phys. Lett. 54A, 452 (1975).

19. T. Ezaki and F. Irie, J. Phys. Soc. Japan 40, 382 (1976).

20. T. Ezaki, K. Yamafuji, and F. Irie, J. Phys. Soc. Japan 40, 1271 (1976).

21. W. E. Timms and D. G. Walmsley, J. Phys. F 6, 2107 (1976).

22. D. G. Walmsley and W. E. Timms, J. Phys. F 7, 2373 (1977).

23. J. R. Clem, Phys. Rev. Lett. 38, 1425 (1977).

24. J. R. Cave and J. E. Evetts, Phil. Mag. B37, 111 (1978).

25. J. R. Cave, Ph.D. Thesis, University of Cambridge (1978).

26. E. H. Brandt, J. R. Clem, and D. G. Walmsley, J. Low Temp. Phys. 37, 43 (1979).

27. J. R. Clem, J. Low Temp. Phys. 38 (to be published).

28. R. Boyer, G. Fillion, and M. A. R. LeBlanc, J. Appl. Phys. (to be published).

29. A. Lachaine, Ph.D. Thesis, University of Ottawa (1976).

30. R. Gauthier, Ph.D. Thesis, University of Ottawa (1976).

31. R. Gauthier and M. A. R. LeBlanc, IEEE Trans. Mag. MAG-13, 560 (1977).

32. P. G. DeGennes, in Superconductivity of Metals and Alloys (W. A. Benjamin, Inc., New York, 1966), p. 59.

33. J. R. Clem, J. Low Temp. Phys. 18, 427 (1975).

34. E. H. Brandt, J. Low Temp. Phys. 28, 263, 291 (1977).

35. J. R. Clem, in Low Temperature Physics - LT14, edited by R. D. Parks (Marcel Dekker, Inc., New York, 1969) Vol. 2, p. 817.

36. E. H. Brandt, J. Low Temp. Phys. 26, 708 (1977).

37. V. G. Kogan, J. Low Temp. Phys. 32, 419 (1978).

38. W. H. Kleiner, L. M. Roth, and S. H. Autler, Phys. Rev. 133, A1226 (1964).

39. A. L. Fetter and P. C. Hohenberg, in Superconductivity, edited by R. D. Parks (Marcel Dekker, Inc., New York, 1968), Vol. 2, p. 817.

40. S. D. Conte and Carl de Boor, in Elementary Numerical Analysis, edited by L. W. Peterson and M. Gardner (McGraw-Hill, Inc., New York, 1965), p. 33.

ACKNOWLEDGMENTS

I would like to express my sincere thanks to Dr. John R. Clem, my major professor, for suggesting the problem and for his remarkable insight, continuous instruction, and constant encouragement throughout the course of this work. Appreciation is extended to Professor Samuel H. Liu and Professor John D. Verhoeven for serving as committee members.

I also wish to thank Mr. Peter S. Li and Mr. Savvas Symeonides for useful discussions of the thesis problem and help with the computer work.

APPENDIX A. DERIVATION OF EQ. (3-18)

Let

$$C_1 = 16\pi A/\kappa^2 \tag{A-1}$$

Since

$$S_{mBO} = r(2m - 1)\tilde{D}_{\|} \tag{A-2}$$

in the limit $\tilde{\xi}_v \to 0$, (3-12) becomes

$$\Delta S_1 = C_1 \sum_{m=m_1+1}^{\infty} K_1[r(2m - 1)\tilde{D}_{\|})]/[r(2m - 1)\tilde{D}_{\|}] \tag{A-3}$$

For $\tilde{D}_{\|} \ll 1$, the sum can be replaced by an integral, and

$$\Delta S_1 \approx (C_1/2\tilde{D}_{\|} r) \int_{y_{M_1}}^{\infty} dy\, K_1(y)/y \tag{A-4}$$

where

$$y = r(2m - 1)\tilde{D}_{\|} \tag{A-5}$$

and

$$y_{M_1} = 2rM_1\tilde{D}_{\|} \tag{A-6}$$

For sufficiently large y_{M_1}

$$\Delta\mathcal{E}_1 \lesssim C_1 \frac{1}{2\tilde{D}_{\|} r y_{M_1}} \int_{y_{M_1}}^{\infty} dy\, K_1(y)$$

$$= (4\pi A/r^2 M_1 \kappa^2 \tilde{D}_{\|}^2) K_0(2rM_1\tilde{D}_{\|}) \tag{A-7}$$

which is Eq. (3-18).

APPENDIX B. DERIVATION OF EQS. (3-20) AND (3-21)

Let

$$C_2 = 8\pi^2 A/(\kappa^2 \tilde{D}_{\parallel}) \tag{B-1}$$

In the limit that $\tilde{\xi}_v \to 0$,

$$LS_4 = -C_2 \sum_{n=1}^{\infty} \cos(n\Delta\alpha_k)\exp(-rn\tilde{D}_{\perp})$$

$$= -C_2 \, \mathrm{Re} \sum_{n=1}^{\infty} \exp(n(i\Delta\alpha_k - r\tilde{D}_{\perp}))$$

$$= -C_2 \frac{\exp(r\tilde{D}_{\perp})\cos\Delta\alpha_k - 1}{[\exp(r\tilde{D}_{\perp})\cos\Delta\alpha_k - 1)^2 + [\exp(r\tilde{D}_{\perp})\sin\Delta\alpha_k]^2} \tag{B-2}$$

which is Eq. (3-20). In the limit that $\tilde{\xi}_v \to 0$,

$$LS_5 = C_2 \sum_{n=1}^{\infty} n\sin(n\Delta\alpha_k)\exp(-rn\tilde{D}_{\perp})$$

$$= -C_2 \frac{d}{d(\Delta\alpha_k)} \left[\sum_{n=1}^{\infty} \cos(n\Delta\alpha_k)\exp(-rn\tilde{D}_{\perp}) \right] \tag{B-3}$$

By taking the derivative of (3-20) with respect to $\Delta\alpha_k$, we have

$$LS_5 = (8\pi^2 A/\kappa^2 \tilde{D}_{\parallel})[\exp(2r\tilde{D}_{\perp}) - 1]\exp(r\tilde{D}_{\perp})\sin(\Delta\alpha_k)/$$

$$\{[\exp(r\tilde{D}_{\perp})\cos\Delta\alpha_k - 1]^2 + [\exp(r\tilde{D}_{\perp})\sin\Delta\alpha_k]^2\}^2 \tag{B-4}$$

Thus, Eq. (3-21) is derived.